



MSU Graduate Theses

Spring 2018


Development of Endogenous Tagging Plasmids for Characterization of Protein Interactions, Localization, and Post- Translational Modifications of Tetrahymena Thermophila Rad23

Evan Andrew Wilson

Missouri State University, Evan3@live.missouristate.edu

As with any intellectual project, the content and views expressed in this thesis may be considered objectionable by some readers. However, this student-scholar's work has been judged to have academic value by the student's thesis committee members trained in the discipline. The content and views expressed in this thesis are those of the student-scholar and are not endorsed by Missouri State University, its Graduate College, or its employees.

Follow this and additional works at: <https://bearworks.missouristate.edu/theses>

 Part of the [Cell Biology Commons](#), [Molecular Biology Commons](#), and the [Molecular Genetics Commons](#)

Recommended Citation

Wilson, Evan Andrew, "Development of Endogenous Tagging Plasmids for Characterization of Protein Interactions, Localization, and Post-Translational Modifications of Tetrahymena Thermophila Rad23" (2018). *MSU Graduate Theses*. 3268.

<https://bearworks.missouristate.edu/theses/3268>

This article or document was made available through BearWorks, the institutional repository of Missouri State University. The work contained in it may be protected by copyright and require permission of the copyright holder for reuse or redistribution.

For more information, please contact bearworks@missouristate.edu.

**DEVELOPMENT OF ENDOGENOUS TAGGING PLASMIDS FOR
CHARACTERIZATION OF PROTEIN INTERACTIONS, LOCALIZATION,
AND POST-TRANSLATIONAL MODIFICATIONS OF
TETRAHYMENA THERMOPHILA RAD23.**

A Master's Thesis

Presented to

The Graduate College of

Missouri State University

In Partial Fulfillment

Of the Requirements for the Degree

Master of Science in Cell and Molecular Biology

By

Evan Andrew Wilson

May 2018

**DEVELOPMENT OF ENDOGENOUS TAGGING PLASMIDS FOR
CHARACTERIZATION OF PROTEIN INTERACTIONS, LOCALIZATION,
AND POST-TRANSLATIONAL MODIFICATIONS OF
TETRAHYMENA THERMOPHILA RAD23.**

Biomedical Sciences

Missouri State University, May 2018

Master of Science in Cell and Molecular Biology

Evan Andrew Wilson

ABSTRACT

Rad23 is a protein involved in both nucleotide excision repair (NER) and proteasome-mediated degradation, and has been suggested to facilitate interactions between these two pathways. The model organism *Tetrahymena thermophila*, which has a transcriptionally silent micronucleus, provides a useful platform for studying the role of Rad23 in global genome NER (GG-NER). However, the ectopic expression systems used thus far in *T. thermophila* to study Rad23 are repressed by UV light and do not account for the background expression of endogenous *RAD23*; these phenomena prevent insightful gains to the true dynamics of Rad23. In this thesis, endogenous tagging cassettes have been designed to allow for the tagging of endogenous *RAD23* or any other *T. thermophila* gene to circumvent the issues inherent to ectopic expression. Additionally, a plasmid has been made to facilitate the genetic knockout of *RAD23* in *T. thermophila*. Basic phylogeny and expression analysis of *RAD23* were also performed to better characterize this protein in *T. thermophila*. The tools designed in this study will aid future researchers in the genetic manipulation of *T. thermophila*.

KEYWORDS: Rad23, Rad4, ubiquitin, nucleotide excision repair, proteasome, *Tetrahymena thermophila*

This abstract is approved as to form and content

Joshua J. Smith, PhD
Chairperson, Advisory Committee
Missouri State University

**DEVELOPMENT OF ENDOGENOUS TAGGING PLASMIDS FOR
CHARACTERIZATION OF PROTEIN INTERACTIONS, LOCALIZATION,
AND POST-TRANSLATIONAL MODIFICATIONS OF
TETRAHYMENA THERMOPHILA RAD23.**

By

Evan Andrew Wilson

A Master's Thesis
Submitted to the Graduate College
Of Missouri State University
In Partial Fulfillment of the Requirements
For the Degree of Master of Science in Cell and Molecular Biology

May 2018

Approved:

Joshua J. Smith, PhD

Randi J. Ulbricht, PhD

Amy E. Hulme, PhD

Julie Masterson, PhD: Dean, Graduate College

In the interest of academic freedom and the principle of free speech, approval of this thesis indicates the format is acceptable and meets the academic criteria for the discipline as determined by the faculty that constitute the thesis committee. The content and views expressed in this thesis are those of the student-scholar and are not endorsed by Missouri State University, its Graduate College, or its employees.

ACKNOWLEDGEMENTS

First, I would like to thank the Missouri State Department of Biomedical Sciences. I feel lucky to have experienced my scientific education in such a supportive and personal atmosphere, where questions are encouraged and help is only a door-knock away. I would like to express my deep gratitude towards Dr. Joshua J. Smith for his empathetic and honest support throughout my career at Missouri State. His efforts during my studies have allowed me to receive an especially insightful perspective to performing science as a career, one that I will utilize and cherish for years to come. I would also like to thank Dr. Randi Ulbricht for mentoring me in my final year; her steadfast assistance saved me from panic countless times and provided me a fresh view of science to expand my paradigm of thinking in the laboratory.

TABLE OF CONTENTS

Introduction.....	1
Guarding the Genome.....	1
Nucleotide Excision Repair (NER).....	6
Recognizing Damage During GG-NER.....	9
GG-NER Regulation via Ubiquitin & Small Ubiquitin-like Modifiers (SUMO) .	11
Ubiquitin at a Glance	15
Small Ubiquitin-like Modifier (SUMO).....	18
Ubiquitin-Proteasome Pathway (UPP)	18
Rad23	24
Rad23 and Transcriptional Regulation of NER.....	29
<i>Tetrahymena thermophila</i> as a Model Organism.....	30
Preliminary Data Regarding Rad23 in <i>T. thermophila</i>	31
Rationale of Endogenous Tagging in <i>T. thermophila</i>	34
Purpose Statement.....	38
 Materials and Methods.....	 39
Plasmid Isolation.....	39
Restriction Enzyme Digestion	40
Dephosphorylation of Digested Plasmid	40
DNA Purification.....	41
Phusion Polymerase Chain Reaction (PCR).....	41
PCR Product Purification.....	43
Ligation of PCR Products into Plasmids	43
Transformation of DH10B <i>E. coli</i> via Electroporation.....	44
Colony PCR	44
Qiaquick® Gel Extraction Kit	45
GeneJET® Miniprep Kit.....	45
GoTaq Green® PCR.....	45
Oligo Phosphorylation and Annealing.....	47
SsoFast™ EvaGreen® Quantitative Real-Time PCR.....	47
pDrive® Cloning	48
Designing Site-Directed Mutagenesis Primers	48
Production of DH10B Electrocompetent <i>E. coli</i>	50
Cryopreservation of <i>E. coli</i>	50
 Results	 51
<i>In silico</i> work on Rad23	51
Optimization of PCR Primers	51
Cloning of tagging constructs	55
Quantitative real-time PCR analysis of Rad23 expression.....	66
 Discussion.....	 67

Future Directions	70
References	74
Appendices	81
Appendix A. Optimization of PCR primers.....	81
Appendix B. Plasmid Maps	84

LIST OF TABLES

Table 1. Primers used in cloning.....	42
Table 2. Epitope tags used in the design of endogenous tagging constructs	46
Table 3. Primers to be used for site-directed mutagenesis of Rad23 K residues	49
Table 4. Domains of Rad23 homologs.	54

LIST OF FIGURES

Figure 1. Overview of DNA damaging agents and insults	2
Figure 2. Major players in mammalian NER	8
Figure 3. Ubiquitin and SUMO-mediated regulation of damage recognition in NER	12
Figure 4. Ribbon structure of ubiquitin.....	16
Figure 5. Overview of ubiquitin and SUMO pathways	17
Figure 6. Structure and function of the 26S proteasome	19
Figure 7. Schematic of UBL-UBA mediated substrate delivery to the proteasome.....	22
Figure 8. Ribbon diagram of Rad23	23
Figure 9. UV phenotype of different yeast Rad23 mutants	26
Figure 10. Deletion of Rad23 UBL domain abrogates post-UV ubiquitylation <i>in vivo</i> in <i>S. cerevisiae</i>	28
Figure 11. TCOFFEE alignments of Rad23 and other ubiquitin chaperone proteins.....	32
Figure 12. UV survival of Rad23 UBL mutants in <i>S. cerevisiae</i>	33
Figure 13. Cells with GFP-RAD23 induced with CdCl ₂ before and after UV treatment. .	35
Figure 14. Rad23 modification after UV damage.....	36
Figure 15. Expression profile of <i>RAD23</i> after UV treatment in <i>T. thermophila</i>	37
Figure 16. Molecular Phylogenetic analysis by Maximum Likelihood method.....	52
Figure 17. 5' to 3' multi-graphical representation of <i>RAD23</i> gene	53
Figure 18. Confirmation digests of the MTTNEO4 construct.....	57
Figure 19. Confirmation of pUC118b::MTTNEO4:BTU2 3'NTS in GM119 <i>E. coli</i>	61
Figure 20. Confirmation of RAD23 knockout plasmid	62

Figure 21. Confirmation of pUC118b::MTTNEO4:BTU2 3'NTS in GM119 *E. coli*.....64

Figure 22. Confirmation of pUC118b::2HA and pUC118b::3XFLAG.....65

INTRODUCTION

Guarding the Genome

Maintaining genomic integrity is essential for robust survival and reliably transmitting genes to future generations. Despite the chemical stability of DNA, damage is an inevitable fact of life. Every day, each cell in the human body must face genomic insults from environmental and endogenous sources. The highly selective pressure to efficiently recognize and repair damage has evolved several distinct repair pathways (Figure 1). The most prominent pathways include mismatch repair (MMR), base excision repair (BER), non-homologous end joining (NHEJ), homologous recombination (HR), and nucleotide excision repair (NER) (Dexheimer, 2013). It is important to note that these pathways are deeply intertwined with transcription and cell cycle regulation, and together these events facilitate the DNA damage response (DDR). Stopping the cell cycle gives time for repair to be completed before the cell begins irreversible processes like DNA replication or cell division, where the damage could become permanent or lethal. Changes in transcription not only provide the cell with a toolkit of proteins to directly carry out DDR, but also help generate feedback loops that ultimately determine whether the cell should survive or undergo apoptosis. This communication between cell cycle progression, transcriptional response, and DNA damage maximizes the chances of surviving genomic insults by preventing non-essential cell processes from depleting energy and resources that could otherwise be allocated to restoring genomic integrity. Despite the importance of whole-cell DDR, this section will focus primarily on reaction

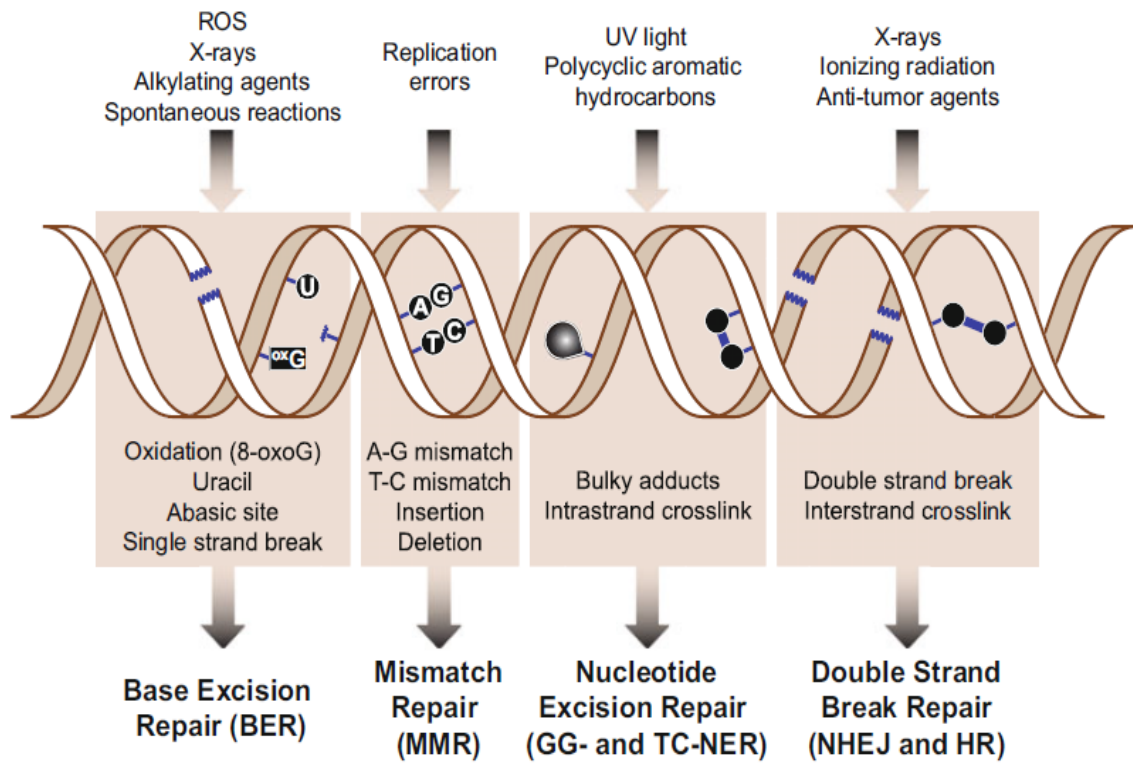


Figure 1. Overview of DNA damaging agents and insults. Each repair mechanism is responsible for fixing specific sub-types of DNA damage, although there is some overlap between each. (Dexheimer, 2013).

pathways that facilitate direct DNA repair. The substrates and mechanisms of the main DNA repair pathways are each briefly discussed below.

Mismatched DNA base pairs can lead to the inheritance of mutation due to the nature of semiconservative DNA replication. Nature has evolved an extremely precise replicative mechanism to minimize DNA mismatches, but even the eukaryotic replisome makes mistakes in the billions of base pairs it copies. MMR decreases this error rate by mending errors that escape the proofreading machinery of the replisome. The complete pathway remains enigmatic in humans, but it is well-characterized in bacteria.

Recognition is performed by homologs of bacterial MutS α , which bind small loop-like DNA on the mismatched strand. MutL α homologues are then recruited in an ATP-dependent manner and create single-stranded nicks upstream and downstream of the mismatch. This positional coordination of nicks with recognition factors allows the cell to distinguish which strand has the incorrect base. Exonuclease activity removes the damage strand, creating ssDNA that DNA polymerase III uses as a template during re-synthesis. The nicks are sealed by DNA ligase, restoring the DNA to a healthy state (Hsieh & Yamana, 2009).

Double-stranded breaks (DSBs) are a severe type of damage that can arise from ionizing radiation or from excessive torsional stress to DNA. Free chromosome ends resulting from DSBs can induce chromosomal fusions, aberrant recombination, or even apoptosis if left unrepaired. The main avenue by which cells repair DSBs is NHEJ. NHEJ begins with the Ku70/80 heterodimer binding to each free dsDNA end, acting as scaffolds to which different NHEJ proteins can be tethered, conferring NHEJ with the ability to manage multiple types of damaged ends. DNA protein kinase catalytic subunits

(DNA PKcs) are then recruited to help align the free DNA ends, which subsequently undergo trans-autophosphorylation, and then recruit a sub-set of end processing factors. Artemis is the usual suspect in vertebrates, and its exonuclease activity resections the free DNA ends so that they can be efficiently ligated together by XRCC-4/DNA ligase IV (Dexheimer, 2013). Although the end-trimming/ligation step can often generate indel mutations, it is far more detrimental for the cell to leave dsDNA ends unrepaired. It is possible for cells to accomplish error-free repair of DSBs through the more sophisticated mechanism of HR, but requisite conditions must be met.

HR can faithfully repair DSBs by using a sister chromatid as a repair template. This stipulation precludes the use of HR outside of the late S and G2 phases of the cell cycle, as these are the only periods when the cell contains duplicated chromosomes to serve as repair templates. HR begins when the MRN complex (composed of Mre11, Rad50, and Nbs1) binds directly to free DNA ends and helps activate the ATM kinase, which helps slow the cell cycle to ensure the DSB(s) are repaired before cell division. Nucleases trim back the 5' ends of the free DNA ends, leaving a 3' ssDNA overhang to which the heterotrimeric replication protein A (RPA) directly binds. Rad51 monomers form a nucleofilament around the overhangs and mediate strand invasion, a process where the 3' overhang displaces the non-template strand of the homologous sequence in the sister chromatid forming a structure known as a D-loop. The displaced non-template strand (non-invading) 3' overhang, creating a large chromatin complex known as a Holliday junction. DNA polymerase η use the templates to add nucleotides to the 3' ends, and it is here that any nucleotides lost during damage are re-incorporated into DNA. At this point the Holliday junction can be resolved in one of two ways, depending on where

endonucleases cut. One alternative incorporates the original invading strand into the sister chromatid and places the displaced non-template strand in the originally damaged chromatid. The other option results in a recombination event that leaves each chromosome with a staggered, double-stranded splice site (Dexheimer, 2013). Either way, both chromosomes end up with a restored DNA duplex, preserving the information lost during damage.

Aside from improper base pairing and structural damage, chemical alterations to DNA by metabolic side products and exogenous agents threaten genome integrity. Although they cause little physical distress to DNA, modified nucleotides can lead to mutations (e.g. GC to TA transversions) if left unrepaired. DNA bases oxidized by active oxygen species (ROS) are often responsible for this type of damage, but alkylation and methylation of bases are other examples of errant DNA modifications. BER is the pathway responsible for repairing this genre of genomic insult. A modified base is recognized by one of many different DNA glycosylases, each responsible for recognizing only specific sub-types of damage. DNA glycosylases also cleave the N-glycosidic bond between the base and deoxyribonucleotide, creating an apurinic (AP) site. This AP site recruits the endonuclease APE1 which causes a single stranded nick in the phosphodiester backbone. At this point BER can proceed through either long patch (LP) or short patch (SP) BER, depending on which DNA glycosylase is present. In SP-BER, DNA polymerase β fills the single nucleotide gap and XRC-1/DNA ligase III α seals the backbone. In LP-BER, PCNA and DNA polymerase δ synthesize 2-8 nucleotides, creating a flap structure through the displacement of the non-template strand. The flap is removed by FEN1, allowing DNA ligase 1 to seal the backbone and complete repair. The

downstream BER proteins also participate in repairing single stranded breaks (SSBs), as they resemble the single-stranded nicks created by APE1 (Dexheimer, 2013). While BER is the preeminent pathway for repairing non-helix distorting damage, the cell must employ yet another distinct mechanism to repair damage that disrupts the helical nature of DNA.

Nucleotide Excision Repair (NER)

NER maintains the integrity of the genome by removing helix-distorting lesions from chromatin. Ultraviolet (UV) light is the predominant cause of helix-distorting damage, resulting in the formation of cyclobutane pyrimidine dimers (CPDs) and pyrimidine (6-4) pyrimidone photoproducts (6-4PPs). These structures form covalent bonds between adjacent nucleotides that cause torsional strain on the helical structure of chromatin. Polycyclic aromatic hydrocarbons can also create these bulky adducts. If left unrepaired, bulky damage can stall replication forks, risking the formation of single- and double-stranded breaks, cell cycle arrest, and can eventually lead to mutation. Absence of any of the core NER factors results in a rare disorder known as Xeroderma Pigmentosum (XP), where patients typically have extreme sensitivity to sunlight, increased risk for cancer, and occasionally neurological defects (Marteijn, Lans, Vermeulen & Hoeijmakers, 2014). There are two subtypes of NER: global genome NER (GG-NER) and transcription coupled NER (TC-NER). The two pathways use identical repair mechanisms and are thus distinguished solely by their mechanism of damage recognition. TC-NER repairs damage in areas of high transcriptional activity through signaling initiated by stalled RNA polymerase and accessory factors Cockayne Syndrome A and B

(CSA and CSB). In contrast, GG-NER must survey the entire genome and ensure transcriptionally inactive DNA is repaired efficiently. The mechanism of damage recognition will be discussed in detail below.

Although there is still debate regarding the temporal recruitment dynamics of NER factors, the general mechanism of repair has been well-established (Figure 2). After damage recognition, damage verification is important to prevent the cell from wastefully expending energy on false-positive repair substrates. Current evidence suggests that the presence of a lesion affects the enzymatic activity of initial NER factors, creating an auto-regulatory system to confirm that damage is present. Upon recruitment of the multi-protein complex Transcription Factor II H (TFIIH) to a site of damage, the ATPase activity of the XPB subunit provides the energy to dock TFIIH and locally denature DNA (Fuss & Tainer, 2011). This allows RPA to bind the ssDNA and XPA is recruited to the complex. Despite XPA being an essential NER factor, its entire role in NER remains enigmatic. Current evidence shows that XPA facilitates recruitment of downstream NER factors and is itself the target of many regulatory modifications. The XPD subunit then uses ATPase and helicase activity to unwind DNA in the direction of the damage, stalling in the presence of damage. Bona-fide lesions also enhance the XPA-mediated stalling of XPD on damaged DNA. Stalled XPD and XPA demarcate a bubble of DNA that contains damage, thought to aid the positioning of downstream NER factors recruited to damage (Dijk, Typas, Mullenders, & Pines, 2014; Schärer, 2013; Sugasawa, 2016).

Once damage has been verified by the pre-incision complex, the recruitment of downstream excision factors marks the “point of no return,” as the repair must proceed to

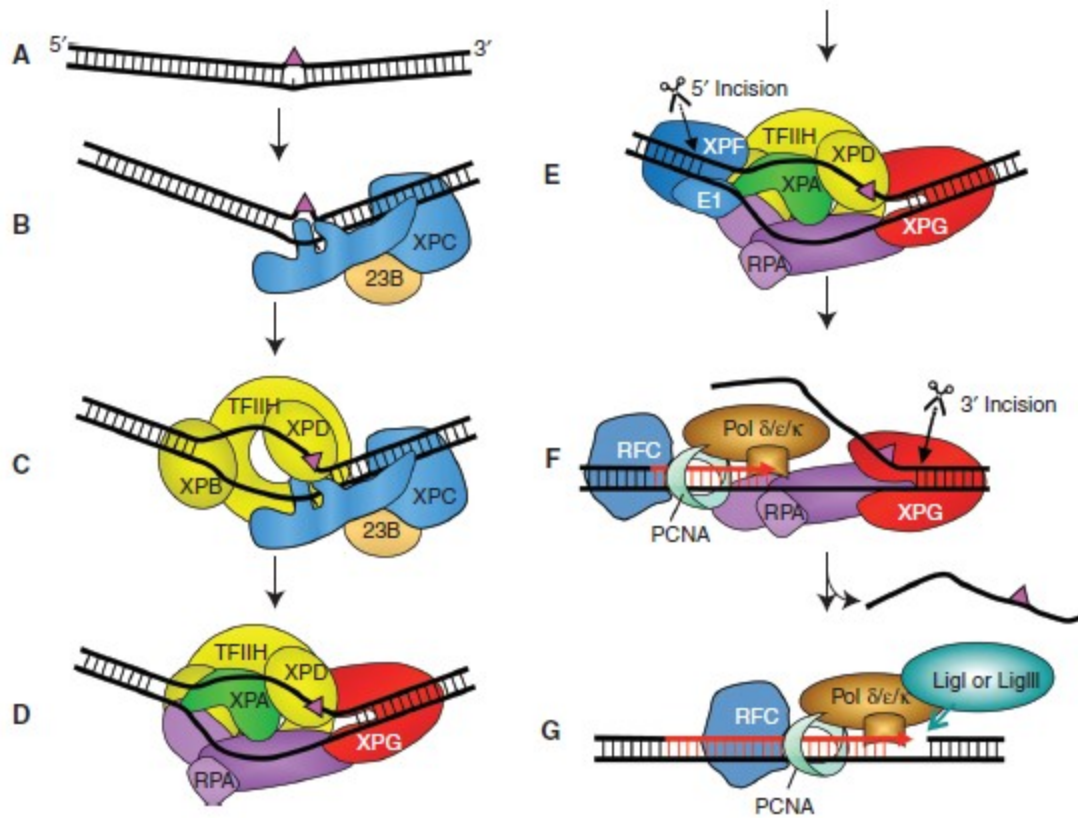


Figure 2. Major players in mammalian NER. (A) Damage (purple triangle) induces a helix distortion that is recognized in (B) by the XPC/HR23B complex. (C) Damage verification and DNA unwinding are facilitated by TFIIH and its helicase subunits XPD and XPB. (D) After final verification of damage by XPA, the 3' incision factor XPG is recruited to the pre-incision complex. (E) After XPF/ERCC1 joins the complex, the 5' and 3' incision facilitate the removal of the damage strand along with TFIIH. (F) Replicative polymerases fill in the gap and in (G) ligase seals the DNA backbone, completing repair. Figure adapted from (Schärer, 2013).

completion once the DNA backbone has been cut. The endonucleases XPF/ERCC1 and XPG make incisions 5' and 3' to the damage, respectively. Once the oligonucleotide containing damage (24-32 bp) has been removed, DNA Polymerase δ or ϵ synthesizes a new strand to reestablish base pairing. The phosphodiester backbone of DNA is sealed by DNA Ligase I or III, resulting in the completion of repair (Schärer, 2013). Although impressive in its ability to remove and repair damage, the true survival value of GG-NER comes from its prowess in recognizing damaged DNA.

Recognizing Damage During GG-NER

Recognizing damage during GG-NER takes the classic “needle in a haystack” dilemma to another level. A more accurate analogy would be searching through six billion pieces of hay and looking for hay that looks *slightly* different than other pieces of hay. This incredible feat is chiefly accomplished by XPC (Rad4 in yeast), although important partners are discussed in the next section. Recognition involves XPC binding to the non-damaged strand and flipping out the damaged bases with a β 3-hairpin domain; this non-specific binding allows GG-NER to remove a variety of helix-distorting lesions (X. Chen et al., 2015). However, XPC has only a small difference in affinity for damaged versus undamaged DNA is similar (particularly CPDs), and XPC has been shown to regularly associate with chromatin in undamaged cells (Sugasawa et al., 2001; Luijsterburg et al., 2010). This creates a paradox: how can XPC efficiently recognize and bind damage across the genome despite a lackadaisical intrinsic ability to bind damage substrates? This conundrum is compounded when considering the additional hurdle of

making chromatin accessible to damage factors. Nonetheless, evolution has developed multiple strategies that provide a solution.

Cells maximize their survival by ensuring that only legitimate damage is processed by NER. The kinetic gating mechanism of damage recognition suggests that initial damage recognition is not governed by the structure of the damage itself, but rather by the probability of XPC to form a stable complex with DNA before dissociating (X. Chen et al., 2015). The presence of damage allows for easier base-flipping by the β 3-haripin domain that encourages formation of the pre-incision complex. This accounts for XPC's observed residency on undamaged chromatin, but does not explain how cells prevent excision of false positive damage errantly recognized by XPC. Further validation is performed by TFIIH, where *bona fide* damage causes a stalling of the XPB and XPD units, leaving a bubbled replication intermediate that facilitates downstream factor recruitment (Li et al., 2015). If the DNA is undamaged, the TFIIH complex does not stall and thus the pre-incision complex collapses. Essentially, the presence of damage increases the residency of repair factors on chromatin, thus providing a platform for the recruitment of subsequent factors.

XPC relies on other proteins to efficiently recognize damage substrates across the entire genome. XPC binds to damage in a complex with HR23B (Rad23 in yeast), and this interaction both stabilizes XPC protein levels and increases XPC affinity for damaged DNA (Bergink et al., 2012; Ortolan, Chen, Tongaonkar, & Madura, 2004). DDB2 (damaged DNA-binding protein 2) specializes in the recognition of 6-4PPs and CPDs, and without this protein cells are extremely deficient in repairing these lesions (Puumalainen et al., 2014). DDB2 simultaneously binds damage and XPC (Sugasawa et

al., 2005) and facilitates chromatin decompaction (Puumalainen et al., 2014), thus helping XPC localize to these damage sites and initiate NER. Aside from their direct assistance in recognizing damage, ubiquitylation events related to Rad23 and DDB2 serve regulatory roles by linking NER to the ubiquitin-proteasome system (UPS). To date, there is no homolog of DDB2 in yeast. However, it could be reasoned that since yeast genome only has two heterochromatic loci outside of telomeres (Miele, Bystricky, & Dekker, 2009), there is less selective pressure to efficiently recognize CPDs, therefore they don't need a DDB2-like protein.

GG-NER Regulation via Ubiquitin and Small Ubiquitin-like Modifiers (SUMO)

The initial steps of NER provide an excellent illustration of how ubiquitin modifications can have a myriad of different outcomes on pathway signaling (Figure 3). After DDB2 binds to sites of UV damage, it activates an associated Cullin-RING containing ubiquitin ligase complex (CRL4), which uses its ubiquitin ligase activity to ubiquitylate targets including XPC and DDB2 (Sugasawa et al., 2005). To our current knowledge, there is no yeast homolog of the mammalian CRL4 complex, but there is a ubiquitin ligase containing Rad16 and Rad7 (NEF4 complex) that is necessary for full UV resistance and has been shown to ubiquitylate Rad4 and Rad23 after UV (Gillette et al., 2006; Ramsey et al., 2004). DDB2 ubiquitylation inhibits its DNA binding capabilities and leads to its degradation. Conversely, XPC ubiquitylation results in *increases* its affinity for DNA (El-Mahdy et al., 2006; Fitch et al., 2003; Sugasawa et al., 2005). However, ubiquitylation is also required for the eventual removal and degradation of XPC (L. Chen, Shinde, Ortolan, & Madura, 2001; Ramsey et al., 2004). The ubiquitin-

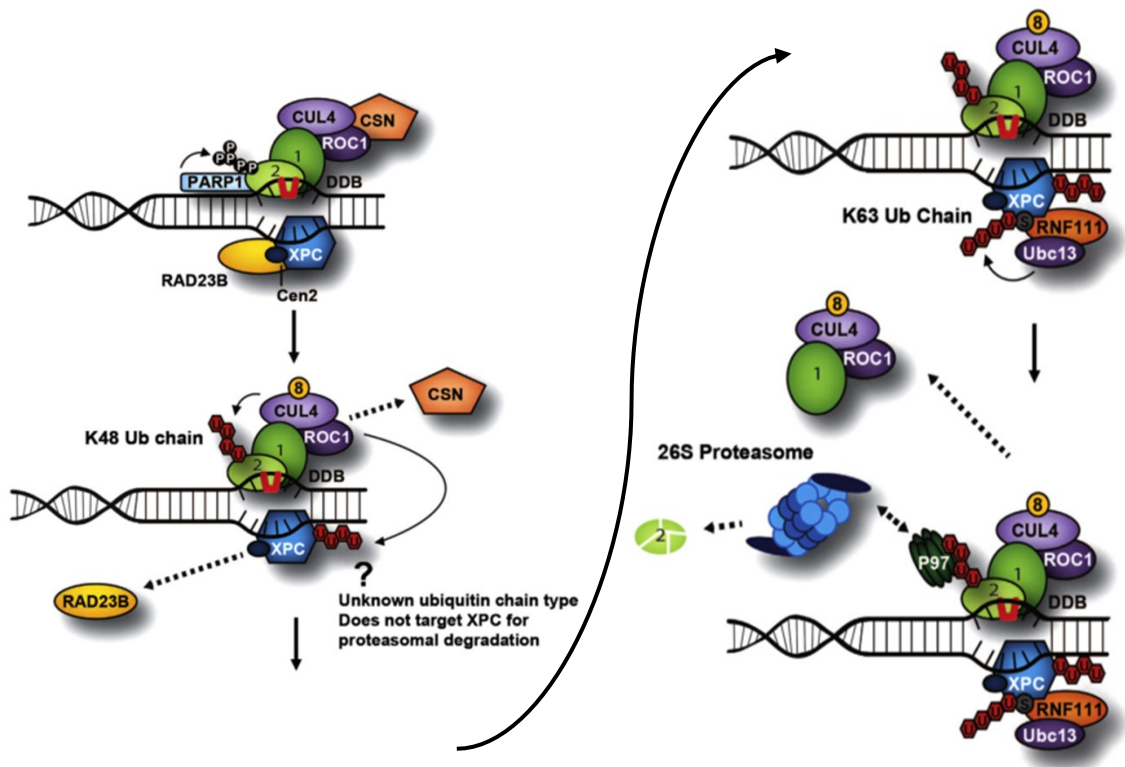


Figure 3. Ubiquitin and SUMO-mediated regulation of damage recognition in NER. See text for discussion of pathway. Figure adapted from van Cuijk et al., 2014. degradation after UV radiation in the absence of USP7 (He et al., 2014).

dependent removal of XPC and DDB2 from chromatin is facilitated by the p97 segregase, discussed next.

The p97 segregase is a hexameric complex that has AAA (ATPase associated with various cellular activities) activity and is thought to disassemble repair complexes to move the NER reaction forward. DDB2 and XPC are removed from sites of damage by p97 (Cdc48 in yeast) in a ubiquitin-dependent manner (Cuijk et al., 2015; Poulsen et al., 2013). The p97/ubiquitin-dependent removal of DDB2 and XPC is required for proficient repair of 6-4PPs and CPDs in human cells (Puumalainen et al., 2014). Removal of XPC from chromatin can be counter-acted by the activity of the de-ubiquitylating enzyme (DUB) USP7, as XPC experiences increased.

Adding a layer of complexity, SUMO and ubiquitin modifications can influence each other through the action of SUMO-targeted ubiquitin ligases (StUbls for short). Previous work has shown that the StUbl RNF111—known to have ubiquitin ligase activity—is responsible for the K63-linked polyubiquitylation of XPC, and this ubiquitylation event is dependent on the E2 Ubc13/Mms2 as well as the initial conjugation of a SUMO group to XPC by the SUMO E2 enzyme Ubc9 (Jackson & Durocher, 2013; Cuijk et al., 2015; Poulsen et al., 2013). Cells lacking this SUMO-targeted ubiquitylation experience a decrease in NER repair efficiency and decreased XPC dissociation from chromatin. The p97/Cdc48 segregase complex has also been directly implicated in maintaining genome stability in a SUMO-targeted manner, acting to disassemble ubiquitylated protein complexes, but not facilitating their degradation (Nie et al., 2012). It is possible that preventing SUMOylation (and therefore ubiquitin/p97 targeting) causes a log jam that prevents downstream NER factors like XPF/ERCC1 and

XPG from localizing to damage efficiently (Cuijk et al., 2015). Although yeast E2 enzymes Ubc13 and Ubc9 have been implicated in regulating NER activity, no yeast homologue of RNF111 has been elucidated (Ramsey et al., 2004).

It is important to note that preventing the ubiquitylation of XPC by CRL4 results in decreased XPC-chromatin interaction, while blocking RNF111-dependent ubiquitylation increases XPC residency on chromatin (Nishi et al., 2009; Poulsen et al., 2013). However, preventing either ubiquitylation event decreases NER repair efficiency just the same. One hypothesis is that the initial ubiquitylation carried out by CRL4 could act to facilitate the hand-off of damage from DDB2 to XPC, allowing recruitment of downstream core factors to the damage site (Sugasawa et al., 2005). Subsequent ubiquitylation of XPC by RNF111 could then remove XPC from the damage site via p97 to allow downstream factors access to damage. Further support for this downstream recruitment hypothesis was shown by Cuijk et al. in 2015. The core NER protein XPG contains a ubiquitin binding motif (UBM), which have a preference for K63 linked chains over K48 linked chains (Burschowsky et al., 2011; Fagbemi, Orelli, & Scharer, 2011); it is therefore tempting to speculate that the K63-linked chain conjugated to XPC by RNF111 encourages the recruitment of XPG to sites of damage. Although many details remain enigmatic, it seems the putative roles of ubiquitin and SUMO in NER revolve around regulating the residency of NER factors on chromatin. Providing spatiotemporal regulation of protein-chromatin interactions helps fine-tune the rates of recognition and repair to prevent spurious NER events that would waste precious energy in times of stress.

Ubiquitin at a Glance

Ubiquitin is a small protein highly conserved in eukaryotes, playing a role in a wide variety of regulatory pathways due to its combinatorial flexibility as a post-translational modifier (Figure 4). Clever proteomic experiments in yeast have shown that over 1,000 proteins are modified by ubiquitin in G₀ cells (Peng et al., 2003). In humans, over 5,000 proteins undergo ubiquitylation (W. Kim et al., 2011). Ubiquitin can be covalently attached to any sterically available lysine residue of a target substrate through the coordinated activity of E1, E2, and ubiquitin enzymes (Figure 5a). E1 enzymes activate free ubiquitin using ATP and subsequently transfer the ubiquitin to an E2. The E2 binds to a cognate ubiquitin ligase, facilitating the transfer of ubiquitin to the target. E2 and E3 ligases have intrinsic ubiquitin conjugating activity, but E3 ligases can also act as scaffolds to which both the E2 and substrate can bind, facilitating the transfer of the ubiquitin group from E2 to substrate. Sometimes the help of an E4 enzyme is required to form poly-ubiquitin chains on target substrates (Ortolan et al., 2000).

Modification via ubiquitin can have a variety of outcomes depending on how many ubiquityl groups are present, where they are located on the target, and the nature of the isopeptide linkages between successive ubiquityl groups. Since all available lysines of ubiquitin have been shown to form chains, the combinatorial complexity of ubiquitin is daunting (Peng et al., 2003). Adding another layer of complexity, this covalent attachment of ubiquitin(s) is reversible, and removal of ubiquityl groups is facilitated by de-ubiquitylases (DUBs). When considering observations of heterogenous chains containing a mixture of ubiquitin and SUMO (discussed below), the ubiquitin system begins to resemble a regulatory snake pit. However, despite the need for further

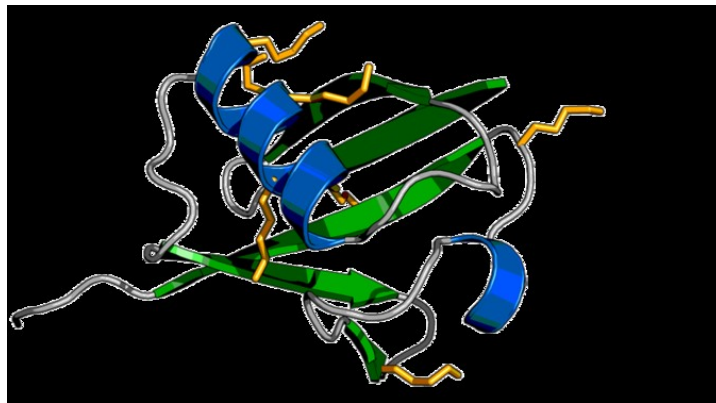


Figure 4. Ribbon structure of ubiquitin. The N- and C-terminus are labeled. Lysine residues are depicted in yellow, with lysine 48 and lysine 63 labeled. In NER, these two lysine residues are directly implicated in the regulation of NER. The conformation of a ubiquitin chain is affected by the lysine linkages within the chain. Figure from (Gordon, Harel, Canner, & Gorrell, 2011).

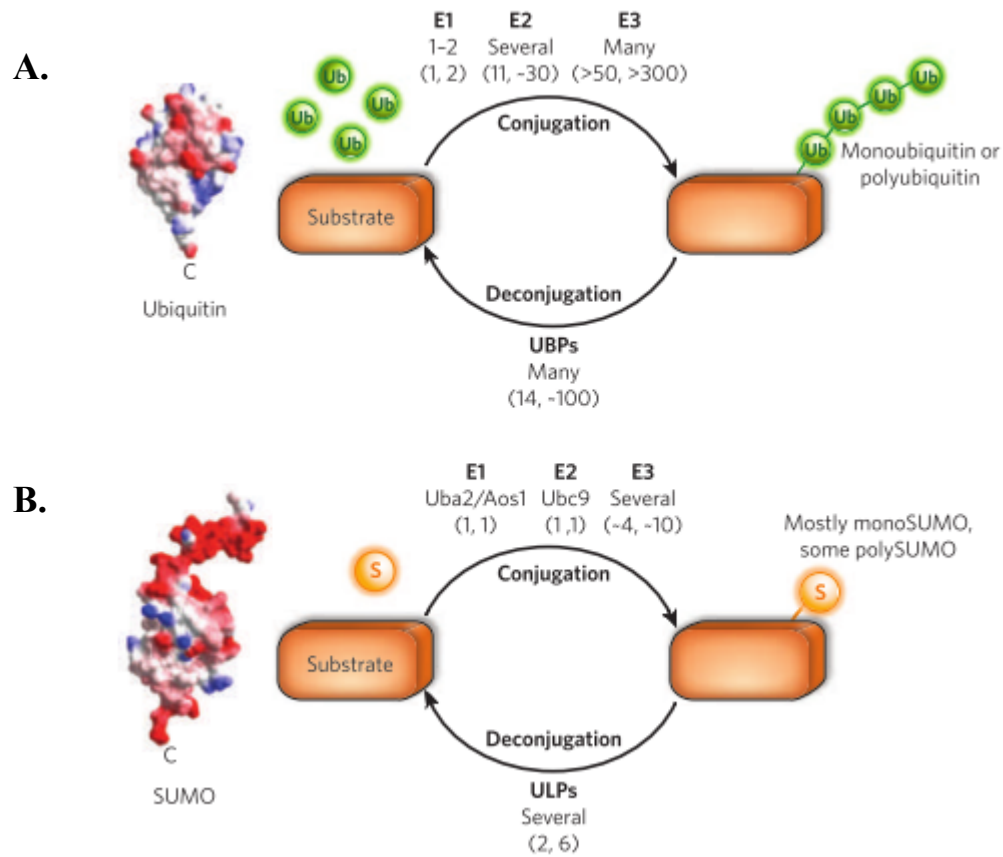


Figure 5. Overview of ubiquitin and SUMO pathways. (A) E1, E2, and E3 enzymes facilitate the attachment of ubiquitin to specific target substrates. Ubiquitin can be removed from targets through the action of ubiquitin proteases (UBP), also commonly known as deubiquitylating enzyme. (B) Overview of SUMO pathway. The SUMOylation pathway is similar to that of ubiquitin, although it has less known enzymes and forms polySUMO chains less often (Bergink & Jentsch, 2009).

investigation regarding the functional implications of chain diversity, the conserved roles of a few well-studied ubiquitin modifications suggest the possibility of a “ubiquitin code” (Komander & Rape, 2012).

Small Ubiquitin-like Modifier (SUMO)

Since the discovery of ubiquitin, SUMO modifications have also gained prominent attention as post-translational modifiers. Like ubiquitin, SUMO is attached to lysine residues of target substrates via the activity of E1, E2, and E3 enzymes and can form poly-SUMO chains (Figure 5b). Although invertebrates have a single SUMO gene known as SMT3 that shares homology with vertebrate SUMO-1, vertebrates also have two additional copies known as SUMO-2 and SUMO-3 (Kamitani, Kito, Nguyen, Fukuda-Kamitani, & Yeh, 1998). SUMO-2 and SUMO-3 share 95% sequence identity with one another and are thus referred to as SUMO2/3. SUMO2/3 shares 50% sequence similarity with SUMO-1 and SMT3, highlighting the evolutionary conservation of this regulatory protein (Hanania, Furman-Matarasso, Ron, & Avni, 1999).

Ubiquitin-Proteasome Pathway

Seminal discoveries regarding ubiquitin have come from research investigating the degradation of proteins by the proteasome in eukaryotes. The proteasome is a 2.5 MDa, multi-protein complex that is primarily responsible for the breakdown of proteins into short amino acid polymers that can be recycled. The proteasome is composed of two

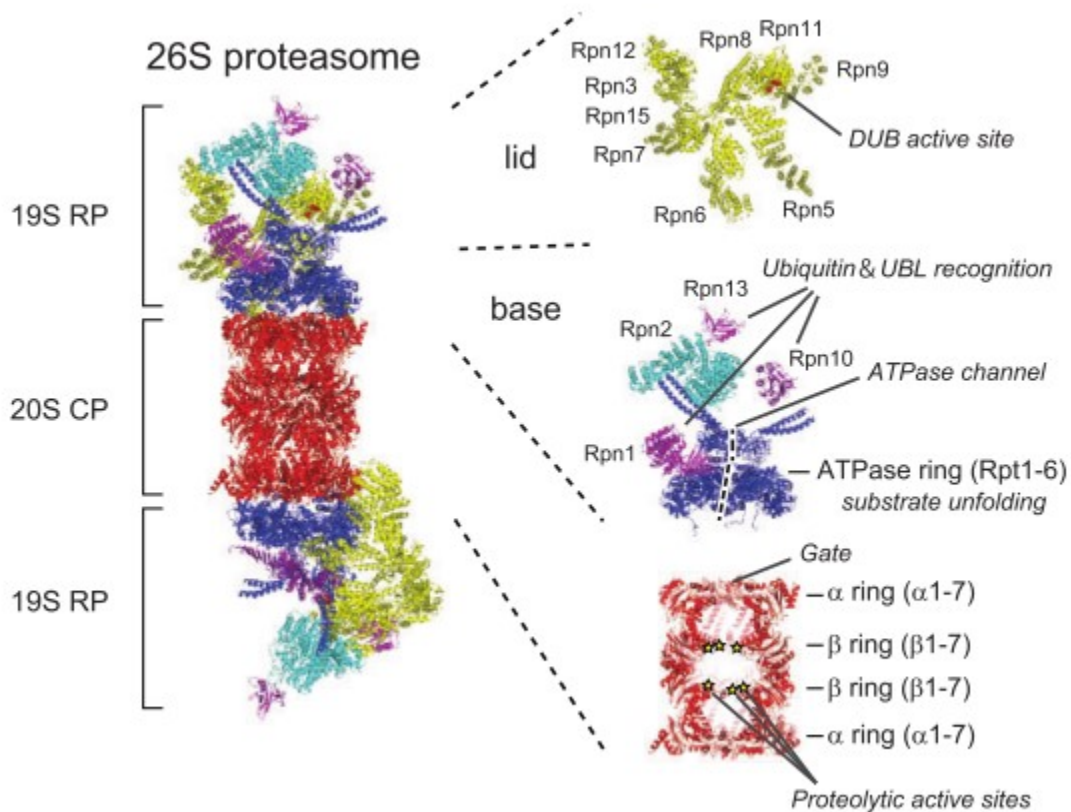


Figure 6. Structure and function of the 26S proteasome. The 2.5 MDa complex is composed of a central 20S core particle (CP) and two 19S regulatory particles (RP). Each RP consists of a lid and base subcomplex; the lid uses DUB activity to remove ubiquitin moieties from substrates and the base recognizes substrates through binding ubiquitin (Rpn10 and Rpn13) and/or UBL domains (Rpn1). The base also contains six ATPases (Rpt1-6) that unfold substrates before they enter the 20S core to be proteolyzed. Figure from Saeki, 2017.

19S subunits that are multiplexed with a 20S catalytic core, together forming 26S proteasome (Figure 6). The 19S caps are responsible for recognizing and unfolding substrates, while the 20S core facilitates proteolysis of peptides. Ubiquitylation is essential for efficient proteasome function because it provides a recognizable tag that can distinguish targets of proteolysis. Substrates with a K48-linked ubiquitin chain of at least four moieties are recognized as degradation substrates (Lowe et al., 2006; Raasi, Orlov, Fleming, & Pickart, 2004). In metazoan cells, the proteasome requires that substrates have a loosely folded sequence (20-30 amino acids) that can act as an initiation region for degradation (Heinen, Ács, Hoogstraten, & Dantuma, 2011), otherwise they must be unfolded before delivery by the AAA-ATPase p97 (Richly et al., 2005). Once bound to the proteasome, ubiquityl groups are removed by DUBs and six AAA-ATPases in the 19S unfold proteins and translocate them into the 20S catalytic core, where peptidases then facilitate degradation (Finley, 2009; Myung, Kim, & Crews, 2001). Since the efficiency of the ubiquitin-proteasome system (UPS) is heavily reliant on proper recognition and delivery of ubiquitylated substrates, cells have developed a variety of functionally overlapping trafficking mechanisms, discussed next.

After a protein has been sufficiently ubiquitylated, it can bind the 19S directly or with the help of a ubiquitin receptor or “chaperone”. Direct ubiquitin binding is primarily done by the 19S subunits Rpn10 (S5a in humans) and Rpn13, each containing ubiquitin interacting motifs (UIM) that bind preferably to ubiquitin polymers (Rosenzweig, Bronner, Zhang, Fushman, & Glickman, 2012). Although Rpn10 and Rpn13 have an avidity for binding ubiquitin, they also have been shown to bind UBL domains (Schmidt, Hanna, Elsasser, & Finley, 2005). Rpn1 shares this ability to bind both ubiquitin and

UBL domains, and even the 19S ATPase Rpt5 (S6a in humans) has been shown to bind ubiquitin (Elsasser & Finley, 2005; Hiyama et al., 1999). Together, this functional overlap between different intrinsic recognition factors of the 19S provides a more robust mode of ensuring targeted substrates are degraded efficiently.

If ubiquitylated substrates do not directly bind a 19S intrinsic factor, they are delivered by ubiquitin chaperone proteins (Figure 7). Ubiquitin chaperones like Rad23 (HR23A/B in humans), Dsk2 (PLIC1-2 in humans), and Ddi1 (DDI1-2 in humans) contain an N-terminal ubiquitin-like domain (UBL) that is highly similar in sequence and structure to ubiquitin (Elsasser & Finley, 2005; Lowe et al., 2006; Raasi et al., 2004). This UBL domain directs these shuttling factors primarily to the Rpn1 subunit of the 19S particle (Rosenzweig et al., 2012; Shi et al., 2016). In addition to the UBL, ubiquitin chaperones also contain one or more ubiquitin associating domains (UBA) that facilitate their binding to poly-ubiquitin chains of target substrates (Heinen et al., 2011; Varadan, Assfalg, Raasi, Pickart, & Fushman, 2005). There is also evidence that UBA domains protect ubiquitin chaperones, allowing them to deliver substrates without being degraded themselves (Heinen et al., 2011). In both *rad23Δ* and *dsk2Δ* cells, proteasome function was reduced, and *rad23Δdsk2Δ* double mutants experienced a further decrease in proteasome function, suggesting these proteins have overlapping but non-redundant functions (Elsasser, Chandler-Mitilello, Müller, Hanna, & Finley, 2004). Loss-of-function mutations in all three ubiquitin chaperones are non-lethal, again emphasizing the robust nature of recognizing ubiquitylated substrates (Saeki, Saitoh, Toh-e, & Yokosawa, 2002; Elsasser et al., 2004).

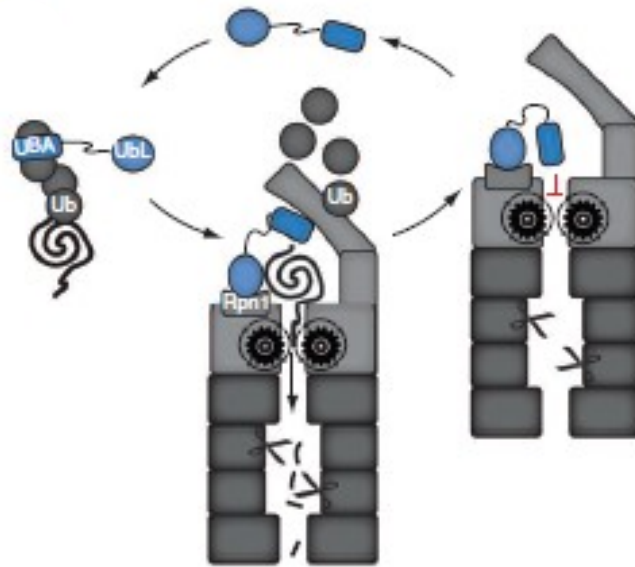


Figure 7. Schematic of UBL-UBA mediated substrate delivery to the proteasome. The degradation substrate (depicted as a black coiled line) is recognized via interaction of the poly-ubiquitin chain with the UBA domain of a ubiquitin chaperone. The interaction between the N-terminal UBL domain and the Rpn1 subunit of the 19S RP brings the substrate in close enough proximity to the DUB and unfoldase activity to initiate degradation. The C-terminal UBA domain prevents degradation of the ubiquitin chaperone so that it can be recycled to repeat the process of delivery. Figure adapted from Heinen et al., 2011.

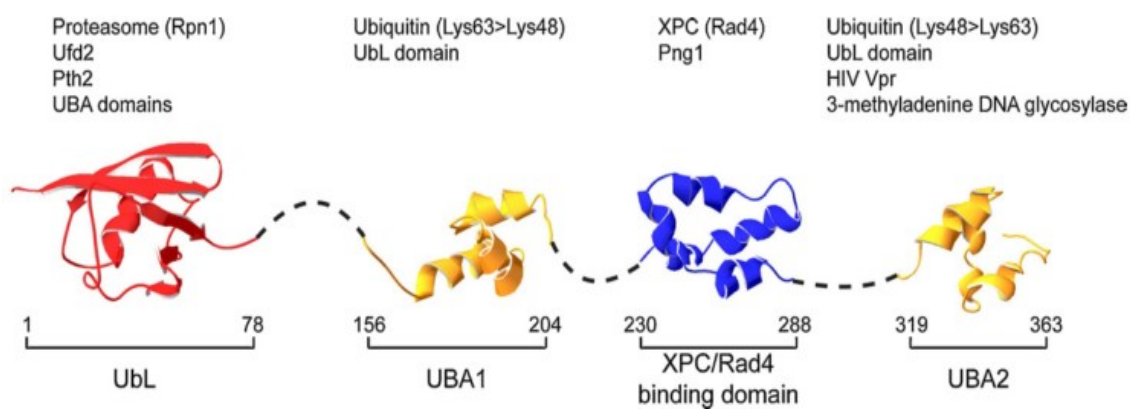


Figure 8. Ribbon diagram of Rad23. Each functional domain lacks catalytic activity, but their distinct and diverse binding dynamics result in the multi-functional nature of Rad23 activity. Putative binding partners are listed above the domain with which they interact. More recent findings have shown that Rad23 has a strong preference for K48 chains (Tsuchiya et al., 2017). Linker regions (shown as dotted lines) confer conformational flexibility that promotes various intermolecular interactions as well as intramolecular interactions between the UBA and UBL domains. Figure from Dantuma, Heinen, & Hoogstraten (2009).

Rad23

Rad23 is a 400-amino acid protein that contains four functional domains. (Figure 8). The internal Rad4-binding domain (R4B) is necessary for the well-established role of Rad23 in the stabilization of Rad4 (yeast homolog of human XPC) (Ortolan et al., 2004; Lommel, Ortolan, Chen, Madura, & Sweder, 2002; Gillette et al., 2006).

The two UBA domains of Rad23 preferentially bind poly-ubiquitin chains of 4-6 moieties (Raasi et al., 2004), favoring K48-linked chains over K63-linked and K29-linked chains (Tsuchiya et al., 2017; Husnjak & Dikic, 2012; Varadan et al., 2005). *In vitro* evidence shows that the UBA domains can inhibit proteolysis and ubiquitin chain elongation by preventing ubiquitin's association with the proteasome and E4 enzymes, respectively (Heinen et al., 2011; Ortolan et al., 2000). However, *in vivo* data has definitively shown Rad23 to facilitate the degradation of a large number of substrates by acting as a shuttling factor for the proteasome (L. Chen & Madura, 2002; Glickman et al., 1999; Liang et al., 2014). The C-terminal UBA2 domain protects Rad23 from being degraded by the proteasome when delivering cargo (Heinen et al., 2011).

The N-terminal ubiquitin-like (UBL) domain shares structural similarity to ubiquitin and is critical in mediating the functional interaction between Rad23 and the 19S RP as well as Ufd2, an E4 enzyme that associates with the Cdc48 segregase complex (I. Kim, Mi, & Rao. 2004; Lambertson, Chen, & Madura, 1999). The UBL is also needed for wild type UV sensitivity and is implicated in multiple Rad23 interactions (Lambertson, Chen, & Madura, 2003; Reed & Gillette, 2007; Joshua Smith, unpublished data). Structural analysis of the UBL-UBA protein Dsk2 reveals the underlying mechanism of regulating UBA-polyubiquitin interactions, and a similar mechanism is

likely in Rad23. The UBA domain forms a weak intramolecular association with the UBL in the absence of ubiquitylated substrates, preventing the UBL from docking the proteasome without cargo (Lowe et al., 2006). When Dsk2 encounters poly-ubiquitin chains they out-compete the UBL for UBA binding, allowing Dsk2 to bind poly-ubiquitylated cargo with concomitant exposure of its UBL domain to guide it to the proteasome.

It was originally hypothesized that the sole function of Rad23 in NER is to stabilize Rad4. However, it was shown that simply adding extra Rad4 to *rad23* mutants did not recover full NER functionality both *in vivo* and *in vitro* experiments (Xie, Liu, Zhang, & Wang, 2004). Additionally, expression of a Rad23 mutant that lacked Rad4 binding (R4B) conferred drastic increase in UV resistance compared to full *rad23* Δ mutants, despite a similarly observed decrease in Rad4 stability in this R4B mutant (Ortolan et al., 2004). This suggested Rad23 is performing another distinct function during NER that facilitates full UV resistance.

Later studies showed the interaction between the UBL domain of Rad23 and the 19S RP influence NER and UV survival. Deletion of Rad23 leads to a severe decrease in UV resistance, while *rad23* ^{Δ ubl} mutants have a phenotype between that of *rad23* Δ and wild type cells (Figure 9) (Ortolan et al., 2004; Wade, Poorey, Bekiranov, & Auble, 2009; Joshua J. Smith, unpublished data). UV sensitivity of *rad23* ^{Δ ubl} mutants was rescued by mutating 19S RP ATPase subunits, indicating that the well-established interaction between the UBL domain and 19S helped prevent a novel inhibitory role of the 19S on NER (Gillette et al., 2001, 2006). This inhibitory role of the 19S is independent of proteolysis, as mutations in the 20S core do not inhibit NER activity

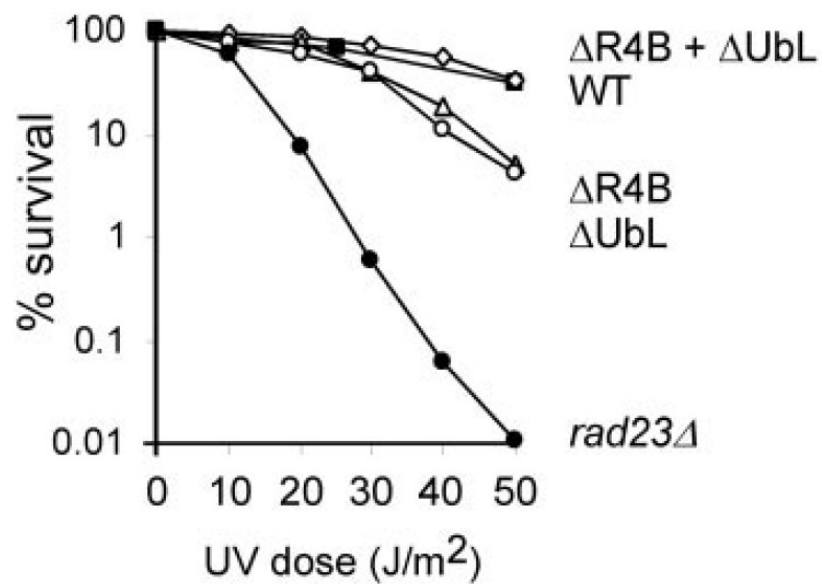


Figure 9. UV phenotype of different yeast Rad23 mutants. Deletion of *RAD23* causes a severe UV defect, while deletion of the Rad23 UBL domain causes intermediate UV sensitivity. Notably, the intermediate phenotype strain only expressing the Rad4 binding domain (R4B) causes a similar UV phenotype to that of Rad23 lacking the entire UBL domain, highlighting the importance of these ubiquitin target sites in the regulation of NER (Ortolan et al., 2004).

(Gillette et al., 2001; Lommel et al., 2002). Further exploration of these functional links between the Rad23 UBL domain, proteasome binding, and NER proficiency provide clues to the mechanisms behind different *RAD23* mutant phenotypes. An interesting discovery came when it was observed that the addition of cycloheximide (an inhibitor of protein synthesis) decreased CPD removal in *rad23Δ* mutants but had no effect on cells lacking the ubiquitin ligase activity of the NEF4 complex (Gillette et al., 2006). This suggests that Rad23 plays a role positively regulating NER that is independent of protein synthesis, while the Rad16/Rad7 ubiquitin ligase activity requires *de novo* protein synthesis to facilitate its positive effect on NER. The same study showed Rad4 was rapidly degraded in *rad23Δ* mutants, but levels remained steady throughout the time course of UV exposure in *rad23Δ* mutants that also lacked the NEF4 E3 activity. This double mutant experienced further decrease in NER efficiency despite having stabilized Rad4 levels. Therefore, it is the ubiquitylation of Rad4, but not its subsequent degradation, that had a correlation with WT cell survival following UV damage. This leads to a model of NER regulation via two different mechanisms: one that involves non-proteolytic activity of the 19S and the Rad23 UBL domain, and the other involving the E3 ligase activity of NEF4 acting on Rad4.

Regulation of Rad23 NER activity is heavily dependent on the UBL domain. This is in accordance with data showing ubiquitylated forms of Rad23 have been reported in yeast and human cells after UV exposure, and deletion of the UBL domain abrogates the *in vivo* ubiquitylation of Rad23 (Figure 10) (Kumar et al., 1999; Ramsey et al., 2004). With so much evidence emphasizing the importance of UBL interactions in promoting NER, it is a worthwhile pursuit to unveil the mechanism of how modifications to this

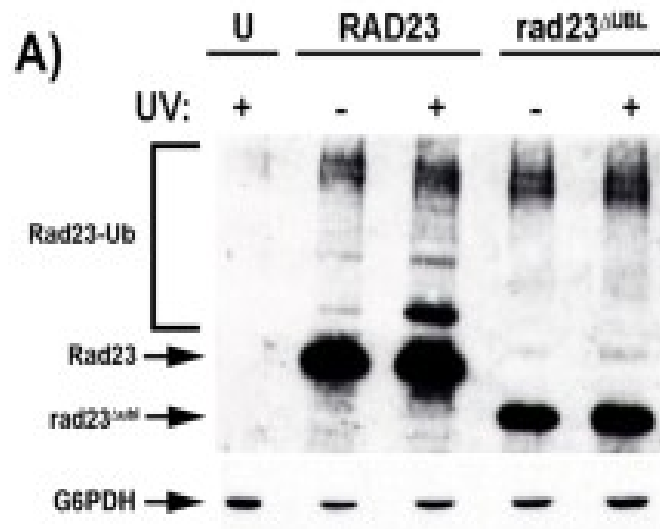


Figure 10. Deletion of Rad23 UBL domain abrogates post-UV ubiquitylation *in vivo* in *S. cerevisiae*. The higher molecular weight species of Rad23 (emphasized by brackets on the left) indicate ubiquitylated forms of Rad23 that become more abundant after UV exposure. Deletion of the UBL domain prevents the ubiquitylation of Rad23 seen in WT cells after exposure to UV light. G6PDH was used as a loading control. Figure adapted with the courtesy of Joshua J. Smith, unpublished data.

domain are functionally linked to changes in Rad23 activity.

Ubiquitin chaperones like Rad23 can recognize short poly-ubiquitin chains better than the intrinsic 19S RP subunits, so Rad23 might provide the cell with a more efficient way to remove NER factors compared to typical proteolysis. Granted, shuttling is the canonical function of Rad23, but the specialized link here is that Rad23 can bind Ufd2—a Cdc48-associated factor—and thus once ubiquitylated complexes have been disassembled by Cdc48, the immediate proximity of Rad23 UBA domains to the poly-ubiquitin chains of segregated substrates facilitates hastier delivery of “spent” NER factors to the proteasome (Bazirgan & Hampton, 2005; I. Kim et al., 2004). With regards to its role in stabilizing Rad4, Rad23 could bind to K48-linked chains on Rad4 to sequester binding sites from Cdc48, allowing Rad4 time to recruit downstream factors before being removed from chromatin. This protective role of Rad23 could also explain the opposing fates of XPC and DDB2 after ubiquitylation in humans.

Rad23 and Transcriptional Regulation of NER

Rad23 regulates transcription of genes both in conjunction with Rad4 and independently. In the absence of UV, the Rad23/Rad4 dimer inhibits the expression of genes that regulate dNTP synthesis, which need to be carefully regulated to ensure an adequate supply of nucleotides are available for repair processes. Upon UV exposure, ubiquitylation carried out by the Rad7/Rad16 ubiquitin ligase facilitates the release of the Rad23/Rad4 heterodimer, relinquishing their repression (Zhou et al., 2015). Another study using mouse cell lines found the XPC/RAD23B complex binds to the Oct4/Sox2 transcription factors to inhibit their influence on genes they regulate (Fong et al., 2011).

Deletion of the *RAD23B* gene in mice does not result in significantly decrease NER efficiency (*RAD23A* can compensate), but it was a curious finding that these mice had severe developmental defects and dysmorphology, suggesting a role of Rad23 in development (Ng et al., 2002). Rad23 has even been shown to affect the transcription of *Rad4*, where *rad23Δ* mutants had decreased levels of *RAD4* transcripts (Gillette et al., 2006). Microarray data have indicated that over 150 UV-responsive genes are dysregulated upon deletion of Rad23, and much of this transcriptional regulation overlaps with that of the 19S RP (Wade et al., 2009). The interactions between Rad23 and the 19S RP could carry functional significance in transcriptional regulation, as the 19S RP has been heavily implicated in non-proteolytic transcriptional regulation in yeast (Ferdous et al., 2007; Maganti et al., 2014). Importantly, these transcriptional activities might have an impact on NER that contributes to the UV phenotypes seen in different Rad23 and 19S mutants.

***Tetrahymena thermophila* as a Model Organism**

Thus far, the scientific community has primarily focused on *M. musculus* and *S. cerevisiae* as model organisms for characterizing Rad23 (HR23A and HR23B in mice). While a useful eukaryotic model, yeast only has a single transcriptionally silent DNA locus (*mat α*), making them a poor model for GG-NER. While mammalian cells have an abundance of heterochromatic regions, the practical hurdles of working with mammalian cells in general costs labs time and money. An overlooked model organism that could provide better insight to NER is *Tetrahymena thermophila*. *T. thermophila* is a binucleated protist that is a more complex eukaryote than *S. cerevisiae*. Due to its

binucleated nature, *T. thermophila* has a transcriptionally silent micronucleus that makes an ideal setting for studying GG-NER. Additional support for its use in research comes from its relatively simple culturing and storage requirements. With a natural habitat in fresh-water ponds, it's no surprise *Tetrahymena* has an easier time surviving *in vitro* than mammalian cells. *Tetrahymena* also has a relatively large size (~20 µm), allowing for easier observation of phenotype using techniques like fluorescent microscopy. Due to these advantages, Rad23 can be more deeply characterized in this organism than yeast, and through comparisons to the multitude of yeast and mammalian studies, we can identify conserved and assumedly essential components of Rad23-related activity in the NER, proteasome, and DDR gene transcription pathways.

Preliminary Data Regarding Rad23 in *T. thermophila*

There is specific evidence that *T. thermophila* is a useful model for studying Rad23. Using the online software TCOFFEE (<https://www.ebi.ac.uk/Tools/msa/tcoffee/>), amino acid sequences were aligned to investigate conservation of the UBL domain residues (Figure 11). There is clear conservation of the lysine residues in the UBL domain between humans and *Tetrahymena*, suggesting the suspected regulation at these sites is a conserved mechanism. This bioinformatics data is corroborated with the unpublished data showing Rad23 is ubiquitylated after UV exposure in *S. cerevisiae* and *T. thermophila* (Figure 10; Joshua J. Smith, unpublished data). Intriguingly, mutating the lysine residues of Rad23 UBL domain to arginine residues severely decreased UV survival in yeast (Figure 12; Shrestha, 2011). It will be interesting to see if performing the same site-directed mutagenesis experiments in *T. thermophila* can replicate these

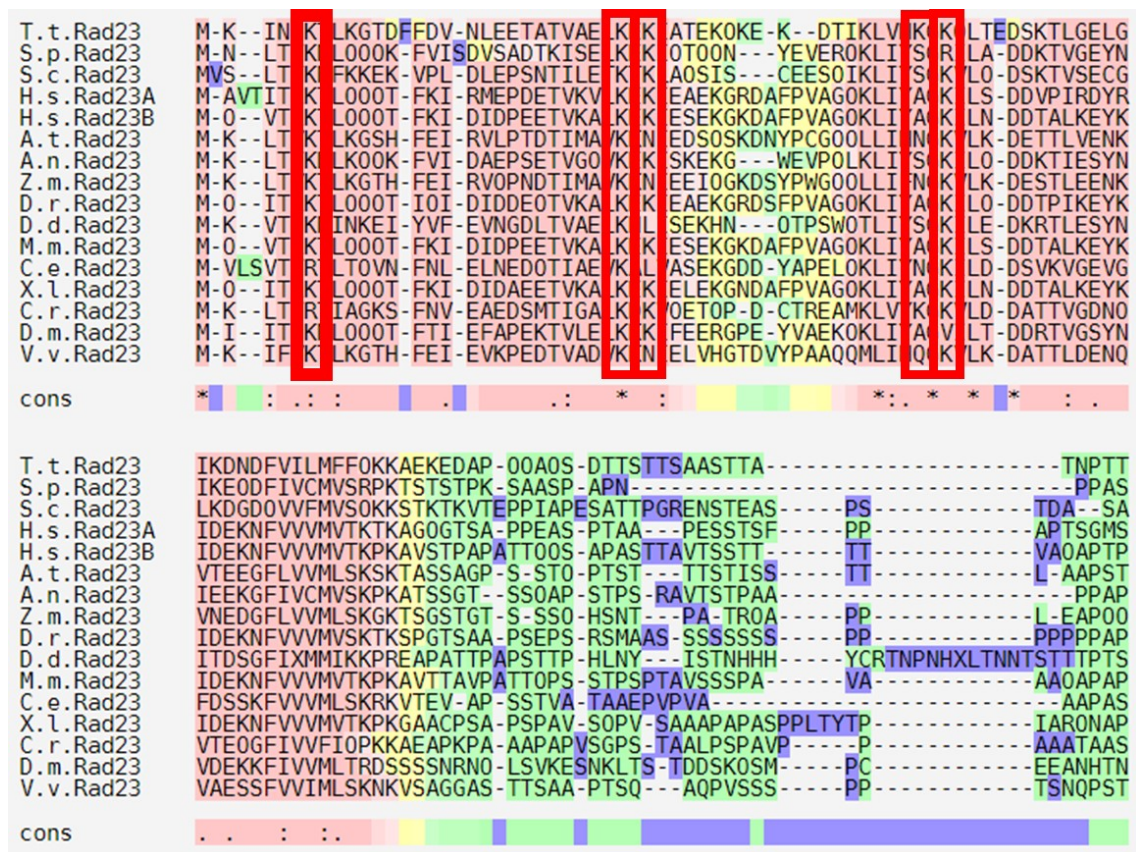


Figure 11. TCOFFEE alignments of Rad23 and other ubiquitin chaperone proteins. Alignments in (A) show the N-terminal region of Rad23, which contains the UBL domain. Red arrows indicate the lysine residues to be mutated using site-directed mutagenesis in *Tetrahymena thermophila*. It is important to note the high degree of conservation at these lysine residues in Rad23 orthologs. Generally, the sequence of the UBL domain is conserved relatively well across the various ubiquitin chaperone orthologs.

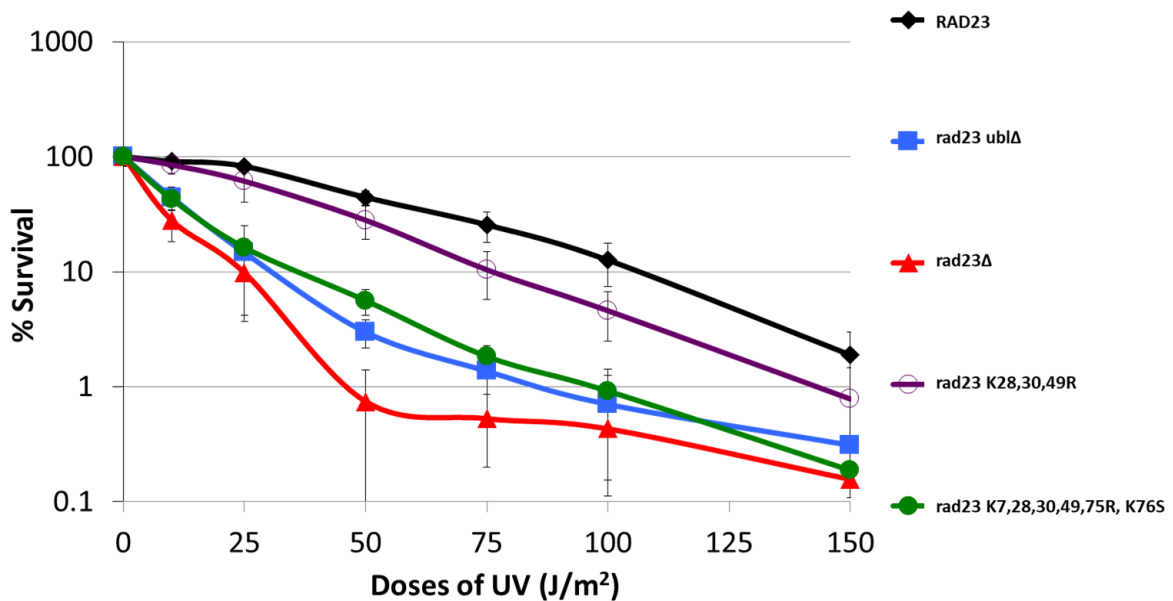


Figure 12. UV survival of Rad23 UBL mutants in *S. cerevisiae*. The sensitivity of Rad23 UBL mutants to the increasing doses of UV is shown. Rad23 deleted cells (red) was highly sensitive to UV, Rad23 with UBL domain deleted cells (blue) resembles to Rad23 UBL mutant (K7,28,30,49,75R, K76S; green); Rad23 WT (black) is not found to be UV sensitive while Rad23 UBL mutant (K28,30,49R) is found to be slightly more sensitive to UV than the wild type Rad23. The values plotted in this graph are the mean of three independent experiments, each performed in triplicates and standard errors are indicated. Figure is from the graduate thesis of Archana Shrestha, 2011.

findings, as it will strongly support the idea of ubiquitylation regulating Rad23 functionality during NER.

An experiment performed by Ariel Carpenter showed that exogenously expressed Rad23 resides primarily in the cytoplasm, but localized to the micro- and macronucleus after UV exposure (Figure 13; Ariel Carpenter, unpublished data). Additionally, *T. thermophila* Rad23 shows no increase in expression following UV (Figure 14). In fact, there is a five-fold decrease in expression following UV (Figure 15), and this might act as a mechanism to compensate for the influx of ubiquitylated Rad23 into the nucleus. It is tempting to speculate that perhaps ubiquitin modifications occurring on the UBL domain or Rad23 are regulating its intracellular localization rather than changes in expression.

Rationale of Endogenous Tagging in *T. thermophila*

While the data regarding Rad23 in *Tetrahymena* are promising, there is a significant caveat concerning the experimental methodology that generated said data. These experiments used RAD23 in exogenous expression cassette under the control of an inducible promoter (MTT1), which can be induced by the addition of cadmium chloride (CdCl₂) to live cells. This cassette was incorporated into a mutated beta-tubulin locus instead of the native RAD23 locus, a strategy that allows for relatively efficient selection of positive transformants in later steps. However, this incorporation into a non-native locus can be detrimental when studying Rad23. A lack of precise transcriptional regulation of this gene leads to an over-abundance of this protein that can saturate proteasome binding sites and alter cellular proteolytic efficiency (Liang et al., 2014). The role of RAD23 in transcription could also be sensitive to its altered expression, risking

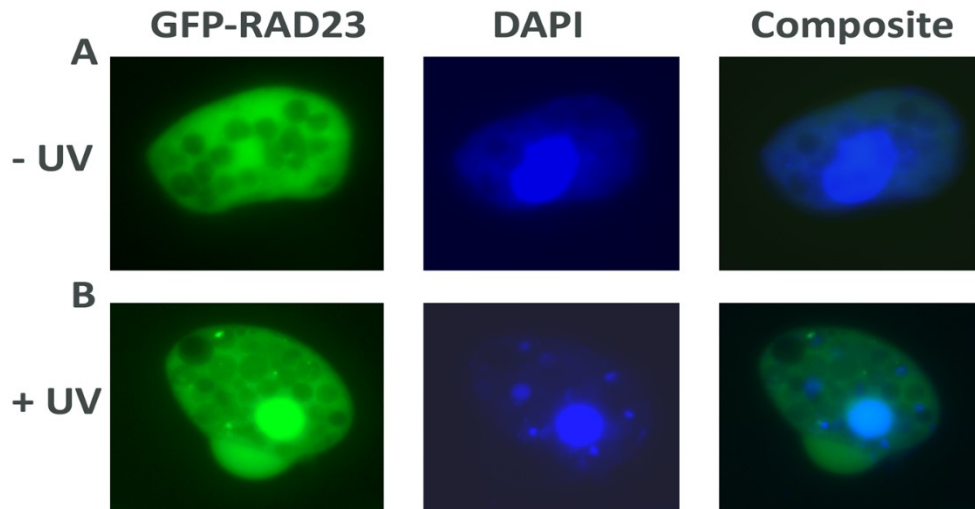


Figure 13. Cells with GFP-RAD23 induced with CdCl₂ before and after UV treatment. Panel A indicates untreated cells with GFP (1), DAPI (2) and composite (3). Panel B indicates UV treated cells with GFP (1), DAPI (2) and composite (3). All cells show expression of GFP however treated cells have a much greater intensity in the nucleus because of global genome repair occurring as response to damage. All cells are shown following one hour of treatment. Figure credited to the unpublished work of Ariel Carpenter.

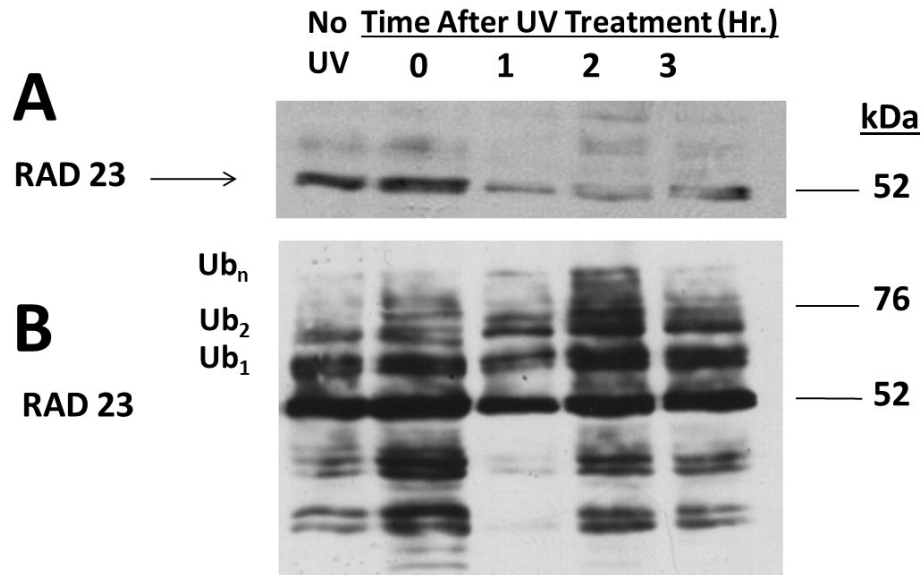


Figure 14. Rad23 modification after UV damage. Exposure at 1 second (A) and 30 seconds (B) of 2HA-RAD23 without induction of ubiquitylation by cadmium chloride. A) Western blot showing the prevalence of unmodified RAD 23 at no and 0 hours of UV treatment, one to three hours after UV treatment it becomes ubiquitylated and the unmodified form decreases. It was shown here that the MTT1 promoter is repressed by UV light, showing decreased expression after UV B) 30 second exposure showing increased repair and ubiquitylation at time of repair. A doublet can also be seen indicating the possibility of a second spliced form of RAD 23. * indicates degraded forms of RAD23. Figure from the unpublished work of Ariel Carpenter.

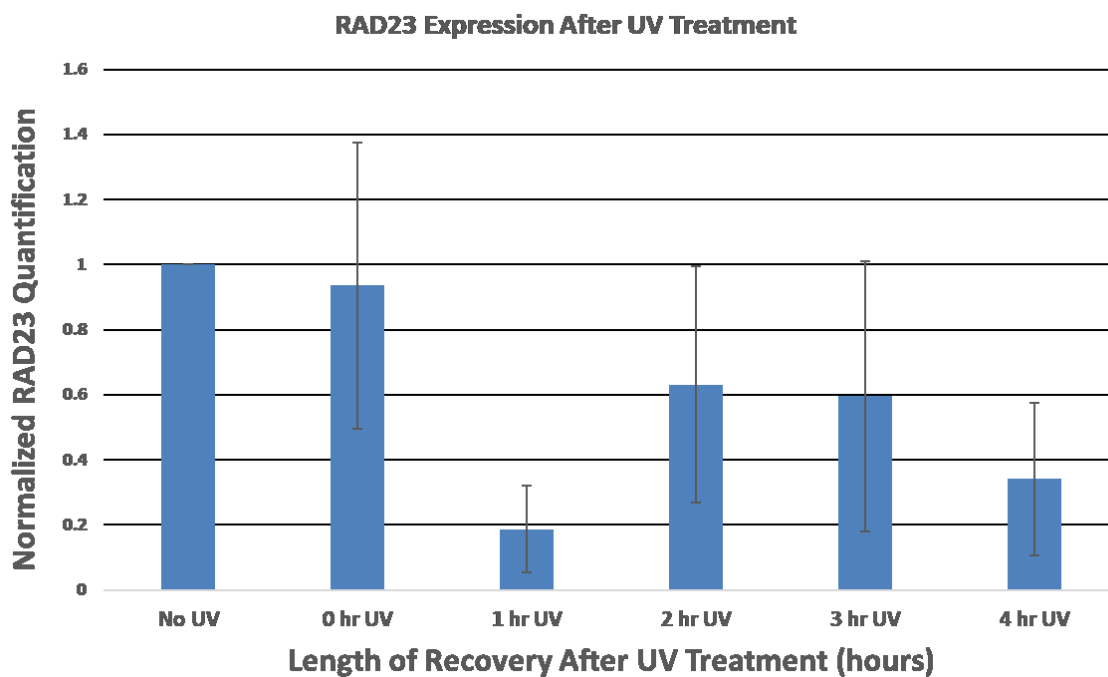


Figure 15. Expression profile of RAD23 after UV treatment in *T. thermophila*. There is a five-fold decrease in the expression of RAD23 1 hr post-UV. Expression is relative to RAD23 expression with no stressor applied. HHP1 was used as a normalization control; ACT1 was used as a quantitative standard.

the chance of a Rube Goldberg-like effect on cellular processes (Krzyszinski et al., 2014; Wade et al., 2009). It has also been observed that the MTT promoter is repressed after cells are exposed to UV light, which is especially inconvenient when trying to study a UV repair-related protein like Rad23 (Joshua J. Smith, unpublished data). A new tagging system needs to be created to circumvent these pitfalls of exogenous tagging. A solution lies in creating an endogenous tagging system for RAD23 (and other genes). By incorporating a tagged version of RAD23 into its native locus, the natural promoter of *RAD23* will regulate expression the expression of tagged *RAD23*, increasing the reliability of data by decreasing the variable impacts of exogenous expression of a gene.

Purpose Statement

This thesis aims to begin the characterization of Rad23 in *Tetrahymena thermophila*. First, data will be collected using online resources to create a foundation of bioinformatics regarding Rad23. The central goal of this thesis is to design tools to endogenously tag *RAD23* and generate specific mutant strains of *RAD23* in *Tetrahymena thermophila* that will provide future researchers with the ability to gain deeper insight to the nature of how the UPS and NER are connected by the functional interactions of this protein. Additionally, expression of wild type *RAD23* in *Tetrahymena thermophila* is assessed under different stressor conditions to provide evidence that the dynamics of this protein's functions are regulated primarily through modifications rather than changes in protein abundance. Finally, primers will be designed for downstream site-directed mutagenesis experiments to introduce key point mutations in the UBL domain of Rad23.

MATERIALS AND METHODS

Plasmid Isolation

Plasmid isolation was used to obtain DNA for screening via restriction digestion (miniprep) as well as generating a larger DNA volume of stock plasmid for cloning purposes (midiprep). The procedures are identical save for the midi-prep increasing all reagent volumes by a factor of 10. The miniprep procedure began when isolated colonies were dotted on a reference plate using sterilized wood applicators and inoculated into 2 mL LB (1% w/v bacto-tryptone, 0.5% w/v yeast extract, 1% w/v NaCl) cultures with 100 µg/mL ampicillin or 50 µg/mL Kanamycin. After 18 hr incubation shaking at 37 °C, each culture was transferred to 1.5 mL Eppendorf tubes and centrifuged at 16,100 x g for 2 min. After decanting the supernatant, the cell pellet was resuspended in 350 µL sucrose lysis buffer (8% sucrose, 0.5% Triton X-100, 50 mM EDTA, 10 mM Tris pH 8.0 in water) followed by the addition of lysozyme (0.625 mg/mL working concentration). After a 5 min incubation at room temperature, the tubes were placed in a 99 °C water bath for one minute to inactivate lysozyme. After 15 min centrifugation at 16,100 x g, the pellet was removed via sterilized toothpick. DNA in the remaining supernatant was precipitated for 5 min using 220 µL isopropanol and 40 µL 3 M sodium acetate, followed by a 10 min centrifugation at 16,100 x g. The supernatant was decanted and the pellet was washed with 1 mL 70% ethanol then centrifuged at 16,100 x g for 2 min. After decanting the supernatant and ensuring the sample was void of any remaining ethanol, the samples were resuspended in 50 µL of 1X TE or sterilized, Millipore water. A 1-3 hr RNase A (10 µg per 100 µL of reaction) treatment at 37 °C followed digestion to remove

remaining RNA. RNase was removed through phenol:chloroform:isoamyl alcohol purification, discussed below. Maps of successfully cloned plasmids are found in appendix B.

Restriction Enzyme Digestion

Restriction enzyme digestion was used to both screen for plasmids (20 μ L reaction volume) and to create compatible ends to facilitate ligation of PCR inserts (200 μ L reaction volume). 20 μ L reaction consisted of 2 μ L 10X Cut Smart buffer (New England Biolabs), 10 units of each appropriate restriction enzyme (New England Biolabs), 4-6 μ g plasmid DNA, and filled to volume with ddH₂O. Reactions were incubated 1-3 hr in 37 °C water bath and exposed to 5 min RNase digestion at room temperature immediately before running the samples on a gel. 200 μ L reactions were composed of 20 μ L 10X Cut Smart buffer (New England Biolabs), 50 units of each appropriate restriction enzyme (New England Biolabs), variable amount of plasmid DNA (depending on necessity of experiment; >50 μ g midprepped DNA), filled to volume with ddH₂O. The reaction tubes were parafilm and incubated in a 37 °C water bath overnight to ensure complete digestion.

Dephosphorylation of Digested Plasmid

To prevent self-ligation of digested plasmids, Antarctic phosphatase (New England Biolabs) was used to remove the 5' and 3' terminal phosphates of the vector. 22 μ L of Antarctic phosphatase 10X buffer (New England Biolabs) was added to the 200 μ L restriction digest, along with 5 μ L of Antarctic phosphatase (New England Biolabs).

After mixing, reactions were incubated at 37 °C for 2 hr to ensure full dephosphorylation. The phosphatase was heat-inactivated during a 5 min incubation at 80 °C. Dephosphorylated DNA was purified using phenol:chloroform:isoamyl alcohol extraction.

DNA Purification

DNA was purified by mixing DNA solution with an equal volume of phenol:chloroform:isoamyl alcohol (25:24:1) and vortexing for 30 seconds. These tubes were spun at 16,100 x g for five min, and the resulting aqueous layer was removed via pipetting and transferred to a fresh Eppendorf tube. DNA was precipitated using 1/10 volume 3.0 M sodium acetate (pH 5.0) and 2.5 volumes 100% ethanol. 1 µL glycogen was added to increase the recovery of small (<1000 bp) fragments. Precipitations were left at -20 °C 4 hr to overnight, then spun at 16,100 x g for 10 min at 4 °C to pellet DNA. The supernatant was discarded and the pellet was washed with 1 mL 70% ethanol, followed by another 10 min at 16,100 x g. The ethanol supernatant was discarded and the pellets were dried until all ethanol was removed. The pelleted DNA was resuspended in sterilized, Millipore water or 1X TE.

Phusion Polymerase Chain Reaction (PCR)

PCR was performed to generate DNA products for cloning. Refer to Table 1 for relevant primer information. PCR was as follows: 0.2 µM final reaction concentration for both the forward and reverse primer, 1.0 unit Phusion polymerase (New England Biolabs, Cat. #M0530S), 1.5 mM MgCl₂, 1.0 M Betaine, 0.2 mM deoxynucleotide triphosphates.

Table 1. Primers used in cloning.

Target Amplified	Forward Primer (5' – 3')	T _A (°C)	Reverse Primer (5' – 3')	RE sites (5'/3')
<i>MTTNEO4</i> (2,033 bp)	ATACGCGGATCCTA GACAATTTATTTCT AAAAAATATTTA	56	GCGTATGGTACCTG CATTTTCCAGTAA AAATTTGAAAAT	BamHI/ KpnI
<i>BTU2</i> 3' NTS (520 bp)	ATACGCTCTAGAG ATCCTTAAATTTAA AATTCAATATAT	55	ATACGCGGATCCCA ACTATATATCAAAT ATAGTGAC	XbaI/ BamHI
<i>GFP</i> (756)	ATACGCCTGCAGG GGGGAGGCGGGGG TGGAAGTAAAGGA GAAGAACTTTTCAC TG	56	GCGTATTCTAGATC ATTTGTATAGTTCAT CCATGCCATGT	PstI/ XbaI
<i>RAD23</i> 5' NTS (1153 bp)	ATACGCGCATGCG CTTTATAAGTATTA ATTTGAGGTTG	59	ATACGCTCTAGATT ATTTTAATGTGTTAT CTTTTAATATA	SphI/ XbaI
<i>RAD23</i> (3,054 bp)	ATACGCGCATGCTT AAGTATATTTTAAA TAATTGAAAAGC	58	GCGTATCTGCAGTT AATACATAAAAATCA TCGTCATCTT	SphI/ PstI
<i>RAD23</i> 3' NTS (1529 bp)	ATACGCGGTACCTT TATTTTGATAGCAC TGTCTTTC	53	GCGTATGAGCTCTT TTTATAGGTTAACA AACAACTTT	KpnI/ SacI

The amount of template DNA varied depending on the type of template DNA: plasmid DNA and *Tetrahymena* gDNA had ~1 µg per reaction, while amplified DNA was in the 0.1 – 1 µM range. Each reaction totaled 50 µL. Refer to Table 1 for averaged primer annealing temperatures. The thermocycler (Bio-rad MJ Mini personal thermal cycler) was programmed with a 1 min denaturation at 98 °C followed by 34 cycles of: 20 s at 98 °C, 30 s at calculated annealing temperature, and 1.5 min at 72 °C. After 34 cycles, the reactions were held at 72 °C for 10 min then held at 4 °C until removal from the machine. Amplified products were visualized via agarose gel electrophoresis to confirm product size and lack of off-target amplification.

PCR Product Purification

To remove PCR buffer components and residual DNA polymerase, PCR products were purified by using phenol:chloroform methods (described above) or using the Promega Wizard® cleanup kit. Protocol was followed according to manufacturer instructions. Samples resuspended in 50 µL nuclease-free water.

Ligation of PCR Products into Plasmids

T4 DNA ligase (NEB) was used to facilitate ligation of digested PCR inserts into compatibly digested plasmids. Totaling 20 µL, the reactions consisted of 2 µL 10X T4 DNA Ligase buffer (NEB), 0.6 µL T4 DNA ligase (NEB; Ligase substituted with water in negative controls), 5 ng vector, variable amount of insert (for larger inserts, a 1:1 or 3:1 molar ratio between insert and vector was used; small inserts used a 5:1 or 7:1 ratio), and filled to volume with water. Controls with and without ligase both did not include

digested PCR products. Reactions were placed in a lidded Styrofoam container with 14 °C water temperature and left 1-2 days at 4 °C before transformation.

Transformation of DH10B *E. coli* via Electroporation

The following protocol was used to transform DH10B electrocompetent *E. coli*. In a chilled 0.5 mL Eppendorf tube, 50 µL of gently thawed DH10B cells were mixed with 1 µL ligation reaction, then transferred into a 2 mm Fisher electroporation cuvette and put on ice until electroporation. The BIO-RAD Gene Pulser II electroporation system was set to the following parameters for electroporation: 2.5 kV, 25 µF, 200 Ω. After the electric pulse, the cells were resuspended in 1 mL LB media then incubated for one hour at 37 °C shaking at 220 rpm. After recovery, typically 100 µL of the culture was plated onto LB plates containing 100 µg/µL ampicillin. After 12-14 hr incubation, colonies were counted then screened for the desired plasmid.

Colony PCR

Colony PCR was used to screen for colonies containing the desired plasmid. Using a sterile toothpick, each colony was swirled into 50 µL sterile ddH₂O. The tubes were boiled for 10 min then centrifuged at 16,100 x g for 5 min. The resulting supernatant was used as a template for the PCR reaction, comprising 10% of the total reaction volume. Using 20 µL reaction volumes, 10 µL GoTaq Green® master mix was combined with 50 pmol of each primer and filled to volume with ddH₂O. Protocol was adapted from the Promega Subcloning Notebook, pg. 50.

Qiaquick® Gel Extraction Kit

Procedure was followed according to manufacture instructions (Qiagen, Cat. #28704) to purify digested DNA fragments separated through gel electrophoresis. Agarose gel was stained, after running, using 200 mL water mixed with 20 μ L ethidium bromide. The gel was placed in shaking container for 15 min followed by a 10 min wash in cold tap water. DNA extracted from the gel was resuspended in 50 μ L 1X TE.

GeneJET® Miniprep Kit

GeneJET® kits were used to facilitate plasmid isolation for screening purposes in times of haste. Manufacturer protocol was followed (ThermoFisher Scientific, Cat. #K0502). The final elution step was performed twice to maximize DNA yield; 1X TE was used as the resuspension solution.

GoTaq Green® PCR

GoTaq Green® (Promega) PCR was performed during colony PCR to screen for colonies containing a desired insert. Reactions were performed according to manufacturer instructions (Promega, Cat. #M7122) using 25 μ L or 50 μ L reaction volumes. GoTaq Green 2X Master Mix (Promega) was combined with roughly 100 ng template or a selected colony (see colony PCR protocol) and 0.4 μ M of each primer, filled to 25 μ L with nuclease-free water.

Table 2. Epitope tags used in the design of endogenous tagging constructs.

Forward Strand (5' → 3')	Epitope Tag	Reverse Strand (5' → 3')
GGGGGGAGGCGGGGGTGGG TGGAGCCACCCGCAGTTCG AAAAATGAT	StrepII	CTAGATCATTTTTTCGAACTGC GGGTGGCTCCATCCACCCCCG CCTCCCCCCTGCA
GGGGGGAGGCGGGGGTGGG TACCCCTACGATGTTCCCGA TTACGCTTACCCCTACGATG TTCCCGATTACGCTTGAT	2HA	CTAGATCAAGCGTAATCGGGA ACATCGTAGGGGTAAGCGTAA TCGGGAACATCGTAGGGGTAT CCACCCCCGCCTCCCCCCTGC A
GGGGGGAGGCGGGGGTGGG GACTACAAAGACCATGACG GTGATTATAAAGATCATGA CATCGACTACAAGGATGAC GATGACAAGTGAT	3XFlag	CTAGATCACTTGTCATCGTCA TCCTTGTAGTCGATGTCATGA TCTTTATAATCACCGTCATGG TCTTTGTAGTCTCCACCCCCGC CTCCCCCCTGCA
GGGGGGAGGCGGGGGTGGG GATTACAAGGACGACGATG ACAAGCATCATCACCATCA CCTACTGAT	Flag6XHis	CTAGATCAGTGGTGATGGTGA TGATGCTTGTCATCGTCGTCCT TGTAATCTCCACCCCCGCCTC CCCCCTGCA

Oligo Phosphorylation and Annealing

Oligos used to construct the different epitope tags generated in this thesis were ordered from Integrated DNA Technologies® (Table 2). Oligos were resuspended in nuclease free water to a concentration of 200 μ M. To prepare oligos for ligation into digested plasmid, 40 μ L phosphorylation reactions were assembled for each tag to be constructed: 29 μ L nuclease free water, 1 μ L of each oligo (sense and antisense strand), 4 μ L 10 mM ATP, 4 μ L 10X polynucleotide kinase buffer (New England Biolabs), 1 μ L T4 polynucleotide kinase (New England Biolabs). Reactions were incubated at 37 °C for 1 hour, followed by a 10-min incubation at 70 °C to denature the enzyme.

Annealing reactions were assembled in 0.5 mL Eppendorf tubes to minimize evaporation during the reaction. 10 μ L of the phosphorylation reaction described above was mixed with 10X SSC (1.5 M NaCl, 0.15 M sodium citrate pH 8.0) and 12.5 μ L water. The reaction was heated to 85 °C for 5 min using a water bath, then heat was turned off and the water was allowed to cool to room temperature. 5 μ L of the annealed, phosphorylated oligos were added to 20 μ L ligation reactions (described above).

SsoFast™ EvaGreen® Quantitative Real-Time PCR

qRT-PCR was performed to assess the expression of *RAD23* under various conditions. RNA was previously isolated from Tetrahymena exposed to specific conditions and reverse-transcribed to cDNA that was to be used as a template in the qRT-PCR reaction. qRT-PCR reactions were assembled in 96-well plates, with each well receiving 19 μ L of the following master mix: 10 μ L SsoFast EvaGreen 2X master mix (Bio-Rad), 0.5 μ L of each specific primer working stock (20 μ M), and 8 μ L nuclease-free

water. 1 μ L of cDNA template was added to each reaction and the plates were briefly centrifuged to ensure reaction components were settled in the wells. Primer information and the respective cDNA targets amplified can be found in Table 1.

pDrive-mediated Cloning

In order to clone the gene encoding NAT, the pDrive cloning system was used (Qiagen, Cat. #231122). Manufacturer protocol was followed, using a 5:1 molar excess of PCR product in the ligation reactions. 1 μ L of the pDrive reaction was transformed into electrocompetent DH10B *E. coli*. Colonies were selected using blue/white screening on LB plates with 50 μ g/mL kanamycin. The presence of NAT was confirmed by performing colony PCR with the M13 F and R primers using the protocol described above. Amplification was visualized using agarose gel electrophoresis.

Designing Site-Directed Mutagenesis Primers

Lysine residues to be mutated in the Rad23 UBL domain were selected based on the work of Archana Shrestha in 2008. Performed *in silico*, select base pair changes to the sequence of the *RAD23* UBL domain mutated lysines 7, 28, 30, 47, and 49 to arginine residues (Table 3). Additionally, these K>R mutations or nearby silent mutations introduced restriction enzyme cut sites that will be used in RFLP-mediated screening for Rad23 UBL mutants. The free, online software WatCut (University of Waterloo) was used to find mutations that would incorporate new restriction enzyme cut sites in the primers without unwantedly disturbing other coding parameters of the sequence.

Table 3. Primers to be used for site-directed mutagenesis of Rad23 K residues.

Rad23 UBL Mutation	Restriction Site for Screening	Oligo sequence (5' – 3')
K7R	BspEI	ATGAAGATCAACATCCGGACTTTAAAGGGCACT
K28R	NruI	TTAGGTTGCTGAACTTCGCGAGAAGATTGCTACTGAAAAG
K28,30R	NruI	TTAGGTTGCTGAACTTCGCGAGAGGATTGCTACTGAAAAG
K47R	SacII	CTATTAAGTTAGTTCACCGCGGAAAATAATTGACCGAAGACT
K49R	ZraI	CTATTAAGTTAGTTCATAAAGGACGTCAATTGACCGAAGACT
K47,49R	SacII	CTATTAAGTTAGTTCACCGCGGAAGATAATTGACCGAAGA

Production of DH10B Electrocompetent *E. coli*

A 1 L culture of DH10B *E. coli* growing in SOB media with 10 mM MgCl₂ was incubated until reaching an OD₅₅₀ between 0.8 and 1.0. Once optimal turbidity was reached the cells were centrifuged at 3000 g at 4 °C for 10 min. Throughout the rest of the procedure the cells were kept on ice or in a 4 °C cold room. After decanting the supernatant, the cells were resuspended in 500 mL chilled, sterilized, deionized, and distilled (ddH₂O). The 10 min centrifugation was repeated, the supernatant was decanted, and the cells were resuspended in 250 mL cold ddH₂O. The 10 min centrifugation was repeated, the supernatant was decanted, and the cells were then resuspended in 20 mL cold, sterilized 10% glycerol solution. The cells were centrifuged again for ten min, and after decanting the supernatant the cells were resuspended in the remaining 1-2 mL of liquid. Aliquots of the cells were frozen using liquid nitrogen and stored at -80 °C. Transformation efficiency was measured as CFU/μg DNA transformed and was calculated using the following equation: (number of transformed cells)/(μg of DNA transformed) x final volume of cell suspension (μL)/volume of cell suspension plated (μL) = CFU/μg of DNA.

Cryopreservation of *E. coli*

For each colony of *E. coli* to be frozen into a stock tube, 2 mL of LB media with proper selective agent (100 μg/mL ampicillin or 50 μg/mL kanamycin) was inoculated using a sterilized wood applicator. After ~18 hr incubation at 37 °C, 700 μL turbid culture was mixed with 700 μL sterilized 50% glycerol in a cryopreservation tube. Cells were flash-frozen using liquid nitrogen and promptly transferred to the -80 °C freezer.

RESULTS

***In silico* work on Rad23**

Before beginning the design of plasmids to be used for endogenous tagging, *in silico* work was performed to establish a context for the project. Characterization of Rad23 in *T. thermophila* began with bioinformatics analysis. The amino acid sequence was obtained from the Tetrahymena genome database (ciliate.org) and used as a query sequence to search for homologs in a wide variety of model organisms using NCBI BLAST. These sequences were then analyzed using ExPASy Prosite (<https://prosite.expasy.org/prosite.html>; Sigrist et al. 2012) to generate Table 4. Using the MEGA 7.0 software, a phylogenetic tree of Rad23 homologs was constructed using the maximum likelihood method (Figure 16). RNA sequencing data for Rad23 was obtained from the Tetrahymena Functional Genome Database (TetraFGD), and it confirms the predicted intron and exon positions given by the 2008 Tetrahymena genome annotation (Figure 17) (Coyne et al., 2008). This agreement is shown by sharp cutoffs of the RNA sequencing data (shown in red) that align perfectly with the predicted exon cutoff points (shown in black), indicating that there were no RNA species detected that were outside the sequence ranges dictated by the exon predictions.

Optimization of PCR Primers

The first step in designing an endogenous tagging vector was to design PCR primers that would both amplify the sequences to be cloned and incorporate terminal restriction sites that would facilitate ligation using complementary overhangs between cut

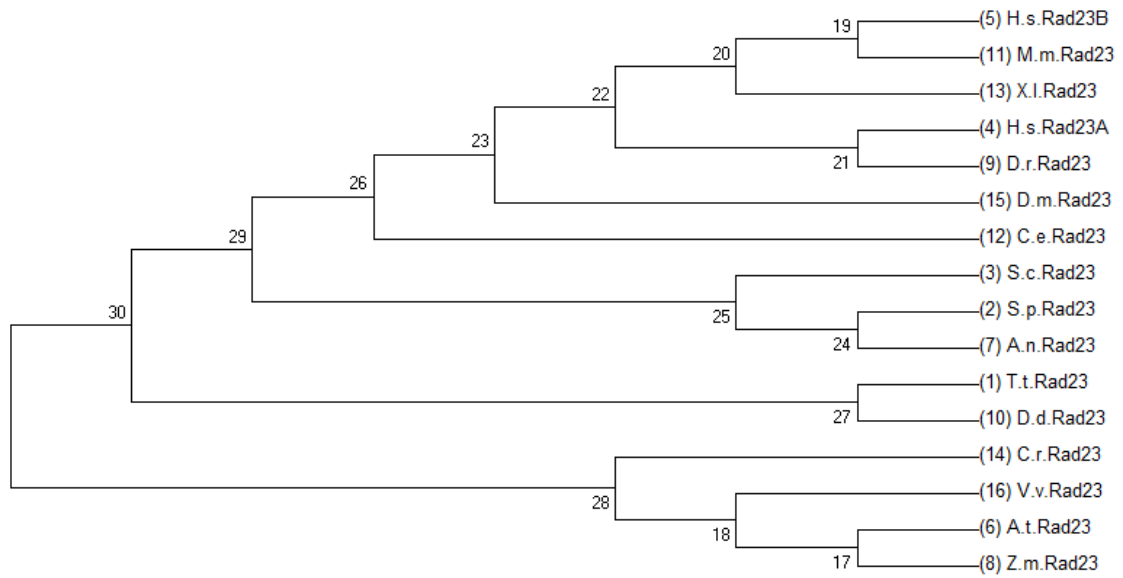


Figure 16. Molecular Phylogenetic analysis by Maximum Likelihood method. The evolutionary history was inferred by using the Maximum Likelihood method based on the JTT matrix-based model. The bootstrap consensus tree inferred from 1000 replicates is taken to represent the evolutionary history of the taxa analyzed. Branches corresponding to partitions reproduced in less than 50% bootstrap replicates are collapsed. Initial tree(s) for the heuristic search were obtained automatically by applying Neighbor-Join and BioNJ algorithms to a matrix of pairwise distances estimated using a JTT model, and then selecting the topology with superior log likelihood value. The analysis involved 16 amino acid sequences. All positions containing gaps and missing data were eliminated. There were a total of 548 positions in the final dataset. Evolutionary analyses were conducted in MEGA7.

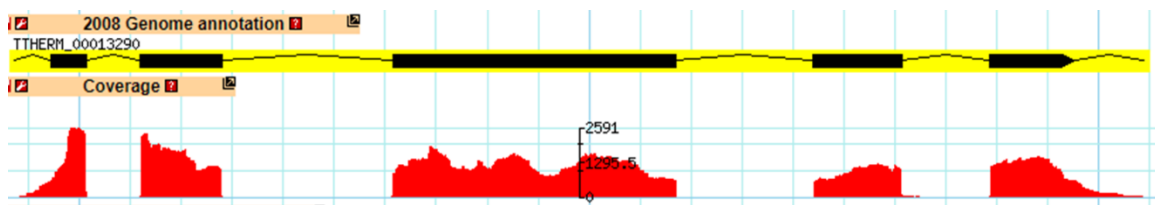
















Figure 17. 5' to 3' multi-graphical representation of *RAD23* gene. Thick black lines correspond to exon sequences and thin black lines correspond to introns. This prediction is based on the 2008 annotated genome of *Tetrahymena thermophila*. The “coverage” sub-tab represents RNA sequencing data. The gaps between red peaks represent introns, as they are spliced out during transcription. Vertical height of the red peaks corresponds with positive expression based on the scale in the middle.

Table 4. Domains of Rad23 homologs*.

Species	Gene Name	Pictorial Representation of Functional Domains	Size (a.a.)	Domain Positions (a.a. #)
<i>T. thermophila</i>	Rad23		373	UBL: 1-78 UBA1: 135-175 UBA2: 271-312
<i>T. thermophila</i>	Dsk2		369	UBL: 5-81 UBA: 323-367
<i>S. cerevisiae</i>	Rad23		398	UBL: 2-77 UBA1: 146-186 UBA2: 355-395
<i>S. cerevisiae</i>	Dsk2		373	UBL: 1-77 UBA: 327-371
<i>H. sapiens</i>	HR23 A		363	UBL: 3-81 UBA1: 161-201 UBA2: 318-358
<i>H. sapiens</i>	HR23 B		409	UBL: 1-79 UBA1: 188-228 UBA2: 364-404
<i>S. Pombe</i>	Rad23		368	UBL: 1-77 UBA1: 135-185 UBA2: 320-360
<i>A. thaliana</i>	Rad23		368	UBL: 1-79 UBA1: 144-187 UBA2: 322-362
<i>D. rerio</i>	Rad23		362	UBL: 1-79 UBA1: 159-199 UBA2: 317-357
<i>D. discoidium</i>	Rad23		341	UBL: 1-76 UBA1: 160-200
<i>M. musculus</i>	Rad23		416	UBL: 1-79 UBA1: 188-228 UBA2: 371-411
<i>C. elegans</i>	Rad23		323	UBL: 3-80 UBA1: 127-167
<i>X. laevis</i>	Rad23		412	UBL: 1-79 UBA1: 191-231 UBA2: 367-407
<i>D. melanogaster</i>	Rad23		414	UBL: 1-78 UBA1: 155-197 UBA2: 370-410

*Data was obtained from ExPASy Prosite (Sigrist et al. 2012)

PCR products and the cut vector. The primer sequences and incorporated restriction sites for each PCR product generated are listed in Table 1. Initial PCR of each target to be cloned was performed using a gradient of different annealing temperatures to find optimal target amplification and ensure absence of off-target amplification (Appendix A).

In addition to primers used for cloning, qRT-PCR primers were made to amplify a non-conserved region of *RAD23* mRNA. A gradient of annealing temperatures was used across four different 25 μ L GoTaq Green® reactions shown in appendix A. Primers were also made to be used in colony PCR to genotypically screen for GFP (Appendix A).

Cloning of tagging constructs

In order to make a tagging construct with the desired characteristics, special cloning inserts were sequentially digested and ligated into a vector. The first insert to be ligated into plasmid would be the MTTNEO4 cassette. It contains a *T. thermophila* codon-optimized NEO gene that encodes resistance to the selection agent paromomycin that is under the control of a metallothionine promoter (*MTTI*), which can be induced by CdCl₂. This will be essential in the selection of properly transformed *T. thermophila* during phenotypic assortment. The next fragment that will be inserted is the BTU2 3'NTS encodes a poly-adenylation sequence that will facilitate proper transcriptional processing of a tagged gene. Appendix B shows plasmid maps of these constructs.

The first construct to be made would incorporate the MTTNEO4 cassette into pUC118b backbone. After preparatory restriction enzyme digestion to create compatible ends between insert and vector, followed by ligation, DH10B cells were transformed, plated on LB agar plates (100 μ g/mL), and screened for the presence of MTTNEO4 using

RFLP analysis. The presence of MTTNEO4 in pUC118b was confirmed using two different digests (Figure 18). The KpnI/BamHI digest excises MTTNEO4 while the BglII digest creates an RFLP that establishes proper directionality of the MTTNEO4 cassette within the plasmid. The colony containing the confirmed plasmid was used to inoculate a 25 mL culture that would be used to create a stock of this bacteria as well as a stock of isolated pUC118b:MTTNEO4, henceforth referred to as pNEO4. The isolated pNEO4 would be used as the recipient vector during the ligation of the BTU2 3'NTS fragment.

Performing PCR of the BTU2 3' NTS fragment was the first major obstacle of this project. A ~100 bp band was present when running a gel of the PCR-amplified BTU2 3' NTS, suggesting the presence of primer dimers (Appendix A). Using the Promega Wizard® PCR cleanup kit failed to remove these erroneous bands, the band persisted throughout a gradient of temperatures and annealing temperatures (data not shown), and gel excision of the BTU2 3'NTS band was failing to yield appreciable quantities of the desired product. Analysis of the primer sequences showed that each primer contained a 5'-terminal sequence of six base pairs that were reverse complements each other. A likely hypothesis is that the primers were annealing to each other in this short region followed by polymerase using the primer sequence as a template for extension. Lowering primer concentrations failed to prevent this small product from accumulating. A new reverse primer was ordered to amplify the BTU2 3' NTS, shown in Table 1. Primer annealing temperature optimization was performed (Appendix A), yielding 59 °C as the temperature to be used when amplifying BTU2 3' NTS.

After the optimized BTU2 3'NTS PCR product was purified, pNEO4 and BTU2 3'NTS were digested with BamHI-HF and XbaI to create compatible ends for the

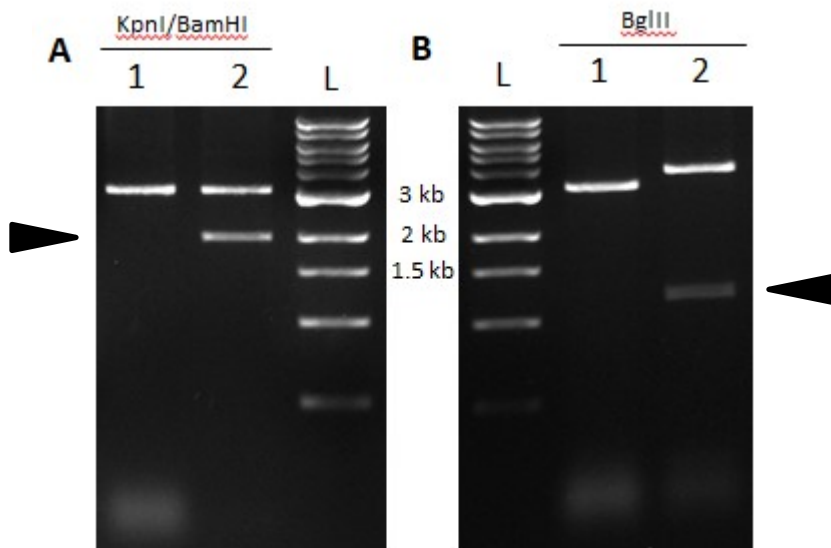


Figure 18. Confirmation digests of the MTTNEO4 construct. (A) The expected agarose gel migration of pUC118b backbone alone (Lane 1) and the MTTNEO4 construct (Lane 2) after digestion with the restriction enzymes *KpnI* and *BamHI*. (B) *BglII* digest of the pUC118b (Lane 1) and MTTNEO4 construct (lane 2) Lane L in both panels contains 1 kb ladder. Bands confirming presence of insert are indicated by black arrows.

subsequent ligation step. After transforming the ligation reactions into *E. coli*, colonies were screened for presence of BTU2 3'NTS using RFLP analysis. No successful colonies were unveiled, even after attempting a pooled screening method that sampled from over 90 colonies. The high background on the positive ligation control plate suggested too much pNEO4 had been self-ligating without insertion of BTU2 3'NTS.

In order to decrease this high presence of background colonies, a lower vector concentration and Antarctic phosphatase was used in the ligation reaction. However, after another round of ligation, transformation, and screen, there were still a high proportion of background colonies in both of the negative controls. After more attempts aimed at adjusting ligation ratios, amount of vector transformed, and ligation reaction conditions, it was decided that something else was causing the trouble with BTU2 3'NTS, as even the fickle nature of ligation-dependent cloning shouldn't generate this much difficulty.

An attempt to work around the BTU2 3'NTS issue came with the plan to first ligate together the XbaI-digested PCR products GFP and BTU2 3'NTS, followed by PCR amplifying the 1.2 kb segment and ligating this fragment into pNEO4 plasmid. Indeed, after optimizing the PCR-from-ligation protocol and performing gel purification of the GFP:BTU2 3'NTS product, this fragment was successfully ligated into pNEO4 and transformed into *E. coli*.

In order to see if the fragment dropping out of the plasmid was the desired GFP:BTU2 3'NTS, XbaI was added to the digestion mixture with the expectation that the observed band would be cleaved into 750 bp and 550 bp pieces representing GFP and BTU2 3'NTS, respectively. When the band failed to show digestion after multiple attempts, it was decided that the XbaI enzyme might have expired and new enzyme was

ordered. Despite the fresh enzyme, it failed to digest the suspected GFP:BTU2 3'NTS band, so the hypothesis generated was that the process of ligation and PCR introduced a mutation into the XbaI cut site and therefore prevented its endonuclease activity.

The digestion, ligation, and PCR of the two fragments was repeated, and upon generating the ~1.2 kb band the product was digested to ensure it had a functional XbaI cut site. After observing successful digestion of the product, the whole GFP:BTU2 3'NTS was ligated into pNEO4. After screening for colonies containing the desired insert, the same phenomena as before occurred where the GFP:BTU2 3'NTS band was excising but it would not itself be digested by XbaI. At this point it became clear that there were other variables responsible for the mysterious cutting activity. After some peer collaboration, it was hypothesized that DNA methylation resulting from the Dam methylase present in DH10B *E. coli* was preventing XbaI from cutting at its restriction site. This was a key discovery that helped move the project forward.

GM119 cells, which lack Dam methylase activity were made electrocompetent and verified to have suitable transformation efficiency using a pUC19 vector. After Undigested pNEO4 and BTU2 3'NTS were each digested with BamHI-HF and XbaI to create compatible ends, followed by a purification step to remove digestion components. The BTU2 3'NTS insert was ligated into pNEO4 and this ligated vector was then transformed into GM119 electrocompetent cells. Screening of positive transformants revealed at long last colonies that contained the desired plasmid (Figure 19), referred to henceforth as pNEO4:BTU2. A midiprep was carried out to provide ample plasmid for the subsequent cloning experiments.

The next step was to create a plasmid that would contain a *RAD23* knock-out (KO) cassette that contained the 5' and 3' NTS of *RAD23* without the coding sequence. Due to the error prone nature of the GM119 strain, the 5'NTS—which is dependent on XbaI cutting—was chosen to be ligated first to minimize the risk of replication errors. The unmethylated pNEO4:BTU2 plasmid as well as purified *RAD23* 5'NTS was digested with SphI-HF and XbaI to create compatible ends for ligation. After transformation and RFLP screening, a colony was found to have the desired insert (Figure 20a). This colony underwent the midiprep procedure to generate plasmid for the ligation step.

With the 5'NTS of *RAD23* successfully incorporated into a plasmid, all that remained for the KO plasmid was the insertion of the *RAD23* 3'NTS just after the MTTNEO4 cassette. Digestion of the *RAD23* 3'NTS and pNEO4:BTU2:5'NTS vector with SacI-HF and Kpn-HF created compatible ends for ligation. After transformation and RFLP screening, a colony was found to have the desired banding pattern showing the *RAD23* 3'NTS dropping out of the plasmid (Figure 20b). This colony was cultured and a glycerol stock was created from the culture for long-term storage.

The non-methylated pNEO4:BTU2 vector was now ready for insertion of different epitope tags and GFP. Purified GFP and pNEO4:BTU2 was digested with XbaI and PstI-HF to create compatible ends for ligation. Meanwhile, the oligomers coding for the epitope tags were annealed and phosphorylated to prepare them for ligation. The epitope tags to be used were 3XFLAG, 2HA, and StrepII. Annealing the individual strands would create terminal overhangs that were compatible with PstI and XbaI sticky ends. Additionally, the digested pNEO4:BTU2 vector was treated with Antarctic phosphatase. The tags were ligated into plasmid and transformed into DH10B cells.

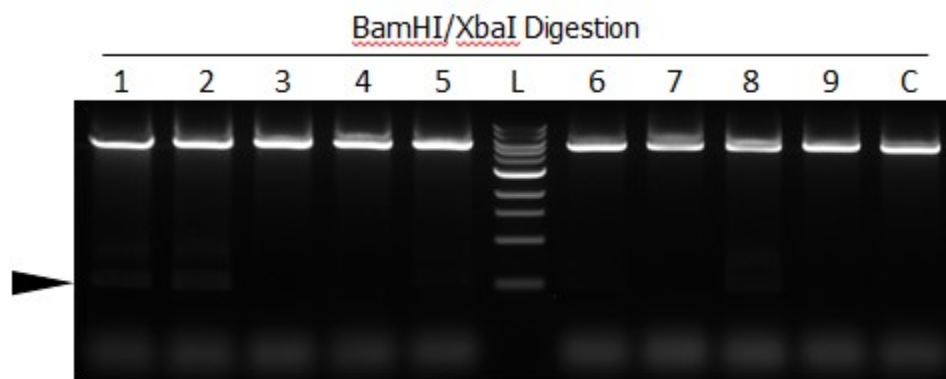


Figure 19. Confirmation of pUC118b::MTTNEO4:BTU2 3'NTS in GM119 *E. coli*. The arrow on the left indicates the roughly 500 bp BTU2 3'NTS fragment dropping out of the plasmid after BamHI/XbaI digestion in lanes 1 and 2. The 1 kb NEB ladder is shown in lane L. C represents a pNEO4 control plasmid lacking the BTU2 3'NTS

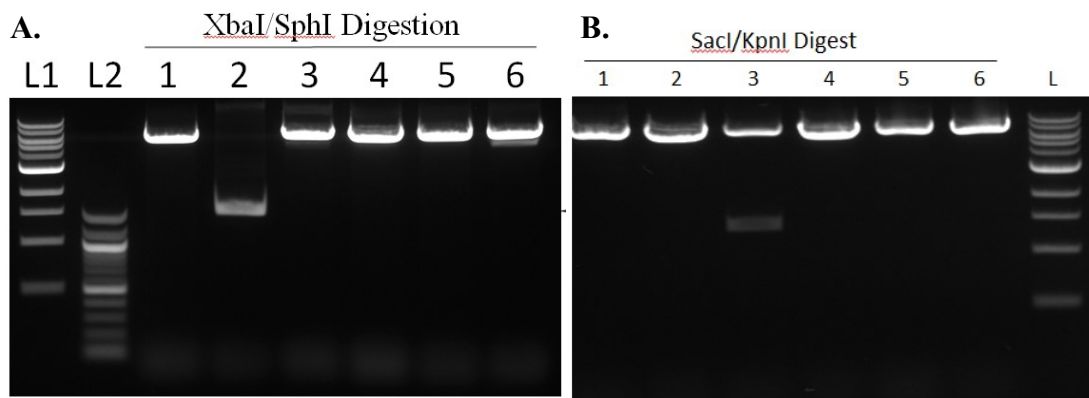


Figure 20. Confirmation of RAD23 knockout plasmid. (A) shows the RAD23 5'NTS dropping out of plasmid in lane 2. The 1 kb ladder is shown as L1, the 100 bp ladder as L2. (B) shows the RAD23 3'NTS dropping out of plasmid in lane 3. The 1 kb ladder is shown in lane L.

Screening of transformed cells was initially carried out using colony PCR for the GFP-containing plasmid (data not shown), but RFLP analysis was used for the final confirmation of the GFP-containing plasmid (Figure 21). Due to the small nature of the tags and methylation of XbaI sites in DH10B, a BamHI/PstI digest was used to excise a fragment containing BTU2 3'NTS as well as the tag. Using BTU2 3'NTS as a size control, excision products that were slightly larger than the BTU2 3'NTS were determined to contain the desired tag (Figures 22a and 22b).

With these “base” plasmids created (containing a tagging cassette for each of the four tags), the next step was to generate cassettes that each had a RAD23 tagged with one of the tags. The cloning process proved difficult, so the decision was made to perform PCR from a ligation reaction to generate the tagged version of RAD23. To begin this process, the RAD23 sequence, generated using PCR, was digested with PstI; the RAD23 3'NTS, also made with PCR, was digested with KpnI; each of the base plasmids were digested with both PstI and KpnI to excise a fragment containing a tag, the BTU2 3'NTS, and the MTTNEO4 resistance cassette (and the plasmid backbone). The purified DNA from each of these reactions was then ligated together using T4 DNA ligase. Using the ligation reactions as templates, PCR was performed across a variety of conditions. Although the amplification of a ~7.5 kb product was observed, there was significant amplification of a ~3 kb fragment. To eliminate this undesired product, gel excision of the high-weight species was performed, and this purified DNA was used as a template in PCR. Due to a broken thermocycler, however, this PCR was not able to be successfully performed.

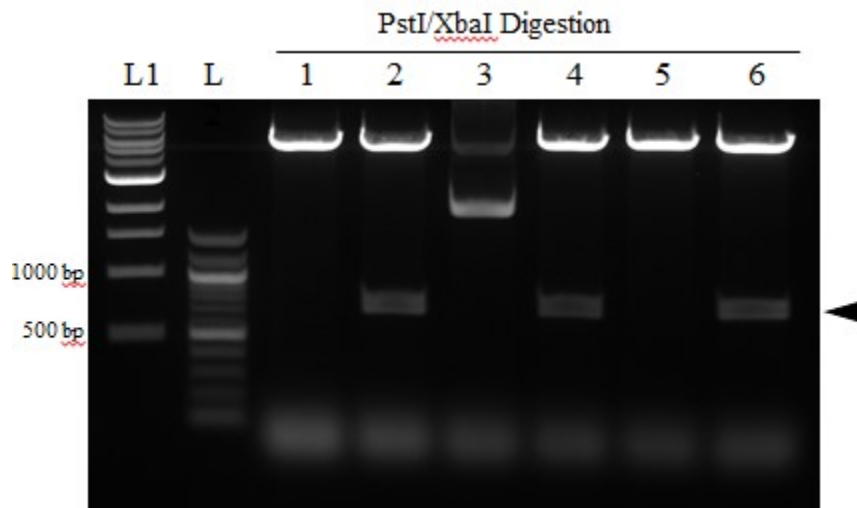


Figure 21. Confirmation of pUC118b::MTTNEO4:BTU2 3'NTS in GM119 *E. coli*. The black arrow on the right indicates the ~750 bp GFP band dropping out of the screened plasmids 2, 4, and 6 after PstI/XbaI digestion. L1 corresponds to the NEB 1 kb ladder, L refers to the NEB 100 bp ladder.

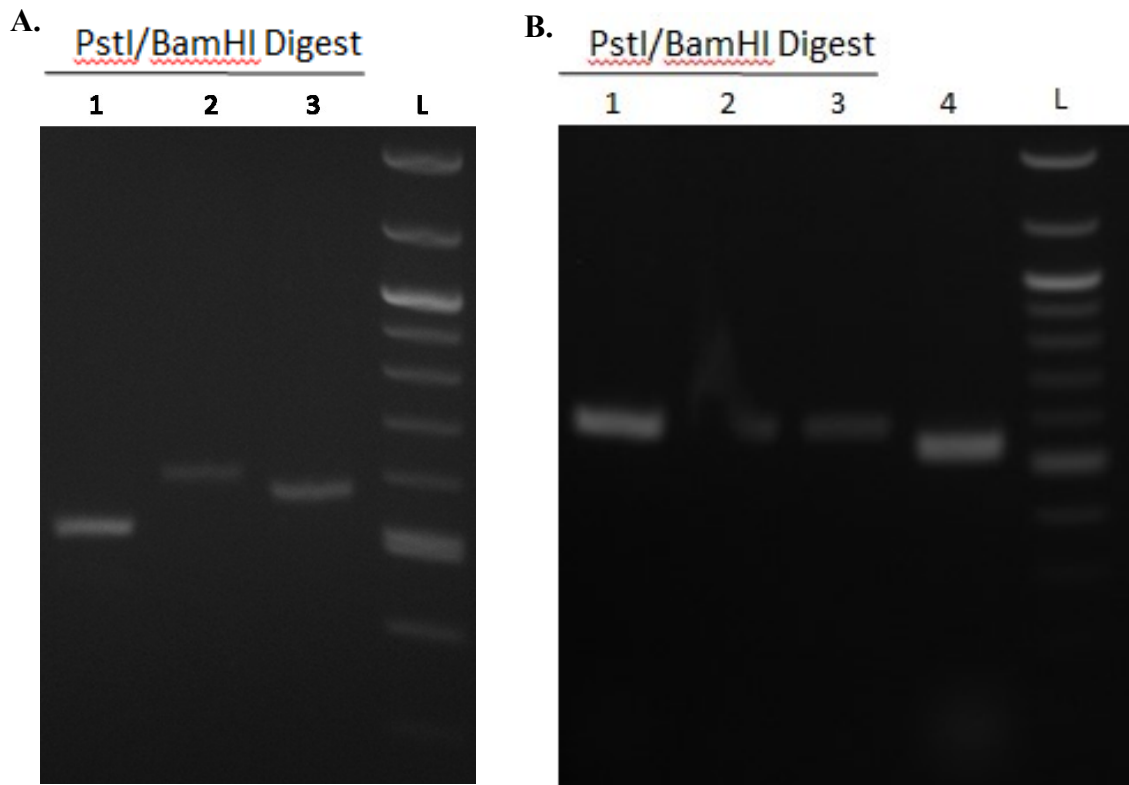


Figure 22. (A) Confirmation of pUC118b::2HA and pUC118b::3XFLAG. Lane 1 was loaded with 5 microliters of BTU2 3'NTS PCR product as a negative control. Lane 2 shows 3XFLAG:BTU2 3'NTS excised from pUC118b::3XFLAG using BamHI and PstI. Lane 3 shows 2HA:BTU2 3'NTS excised from pUC118b::3XFLAG using BamHI and PstI. Lane L is a 100 bp NEB ladder.(B) Confirmation of pUC118b::StrepII. Lanes 1-3 show StrepII:BTU2 3'NTS excised from pUC118b::StrepII using BamHI and PstI. Lane 4 was loaded with 5 microliters of BTU2 3'NTS PCR product as a negative control. Lane L is a 100 bp NEB ladder.

Quantitative real-time PCR analysis of Rad23 expression

The project turned to performing quantitative real-time PCR (qRT-PCR) on *RAD23* expression in *Tetrahymena thermophila*. The aim was to investigate how various stressor conditions affected the expression of Rad23. Hydrogen peroxide (H₂O₂), methyl methanesulfanoate (MMS), and ultra-violet light (UV) were the three stressors applied to vegetative cells. H₂O₂ initiates the BER pathway to remove oxidative damage; MMS causes blanket methylation of DNA, stalling replication forks and causing double-stranded breaks, which in turn initiates double stranded break repair; UV light causes chemical adducts that must be repaired by NER. Investigating scenarios with different but comparably intensive cellular DNA repair activity not only provides more experimental control for the specific changes in Rad23 expression during NER, but also could provide evidence for possible roles of Rad23 in other DNA repair pathways. Rad23 levels were normalized to HHPI (a commonly used housekeeping gene in *Tetrahymena* involved in heterochromatin maintenance) and set relative to baseline Rad23 levels in unstressed cells. Amplification of known ACT1 standards ranging from 0.1 ng to 1000 ng provided data for a standard curve to be used in absolute quantification of mRNA levels. Figure 15 showed that expression of RAD23 does not increase after UV exposure, and there is a five-fold decrease in expression 1 hour after UV.

DISCUSSION

The initial cloning strategy was to perform an “all in one” ligation with digested MTTNEO4, BTU2 3’NTS, GFP, and pUC118b. The probability of successful ligation was much lower due to the multiplicity of ligation products that can form from combining so many fragments into one mixture. Combined with novice research hands at the wheel, this technique failed to produce results and it was decided that the one-by-one methodology would be more efficient due to its reliability. Indeed, the relatively quick success of ligating the MTTNEO4 fragment into pUC118b gave hope of good things to come.

Unfortunately, the underlying issue of XbaI methylation sensitivity plagued this project with unexpected results that were investigated with red-herring hypotheses in mind, culminating in a severe reduction in research progress attained. At first there was a lack of attention paid to the background colonies present on transformation plates, and not using this hallmark indicator of defective restriction enzyme digestion led to unnecessary lab hours. Additionally, the research troubleshooting process was at first plagued with tunnel vision, meaning only one factor would be adjusted at a time before attempting a new ligation. Although this period instigated an exploration of cloning troubleshooting that did help develop my palette of research techniques and resources, the repeated failed ligation attempts were discouraging for me as a scientist. Analyzing these mistakes retrospectively has further instilled the importance of developing thorough, systematic troubleshooting processes that are based on testable hypotheses.

The slow research start in this project was centered on XbaI. At first the lack of cutting was thought to be due to a defective XbaI enzyme, so new XbaI was ordered from New England Biolabs to ensure expired/contaminated enzymes was not a cause of the issues. When cutting was still not observed, it was then hypothesized that XbaI was sensitive to terminal digestion sites, as the product website showed XbaI needed at least four nucleotides present outside of the recognition site to efficiently cut. Sequential digestion was performed, where plasmid was incubated with XbaI alone for six hours, followed by the addition of BamHI to facilitate cutting of the other free dsDNA end.

Disappointingly, the sequential digestion failed to yield positive results. In an attempt to circumvent the issues with XbaI cutting plasmid, GFP and BTU2 3'NTS PCR products were single-digested with XbaI and ligated together. PCR was performed using the ligation reaction as a template to generate this GFP:BTU2 3'NTS product. This ~1.2 kb insert was then ligated into the pNEO4 plasmid, using BamHI and PstI as the enzymes facilitating directional insertion. Although an RFLP screen of colonies transformed with this plasmid showed a GFP:BTU2 band dropping out, XbaI was still not able to cut the 1.2 kb fragment into its constituent parts. Naively, it was assumed that the XbaI site had been mutated during the PCR of the ligated GFP+BTU2 3'NTS fragment.

More backtracking occurred, until it was finally (and correctly) concluded that XbaI was not cutting due to methylation of its cut site. Specifically, XbaI sites are methylated if preceded by a GA or are followed by a TC. Sure enough, this is the case for plasmids created in this project. It was difficult to swallow such a simple answer as the source of my research woes, but the inexorable winds of science pushed me forward. This discovery also helped re-emphasize the importance of peer collaboration; a fellow lab

member (Jeremy Tee) was the person who found an article about XbaI site methylation. When confronted with research challenges, there is a good chance someone else has experienced or heard of the same issue and found a solution. Although sometimes a humbling process, communicating research problems opens a dialogue with peers and mentors that can expedite success.

It was fortunate that Dr. Garrad had a strain of *E. coli* available that lacked Dam methylase, yet again emphasizing the positive role of collaboration in obtaining research success. After making these cells electrocompetent, all the trump card for methylation had finally been attained. Using the plasmid cloned in GM119, BTU2 3'NTS was successfully ligated into the pUC118b:MTTNEO4 construct, followed by each of the epitope tags in Table 2. The potential uses of these plasmids are discussed in the future directions.

FUTURE DIRECTIONS

The utility of this thesis project requires its future application to genetic study in *Tetrahymena thermophila*. The different DNA fragments combined to make these plasmids will each have a specific function to allow for eventual endogenous tagging of *RAD23* (or virtually any other gene using the tag-only plasmids). The primer sequences, annealing temperatures, and the restriction enzyme digestion sites of each fragment discussed below are summarized in Table 1. Green Fluorescent Protein (GFP) will be used as a tag to enable visualization of Rad23 localization via fluorescence microscopy. The *RAD23* sequence encodes the *T. thermophila* genomic sequence of *RAD23* that lacks a stop codon, ensuring that the C-terminal tag will be transcribed as part of the same mRNA as the *RAD23* gene. The *RAD23* segment also contains 1 kb of sequence upstream of the transcription start site to provide homologous sequence with the endogenous *RAD23* to facilitate recombination into the genome. The *RAD23* 5' NTS and *RAD23* 3'NTS will be used to provide homologous sequence that facilitates recombination of the knockout construct into the endogenous *RAD23* locus following transformation. The *RAD23* 3'NTS will also be used in the *RAD23* tagging plasmids to provide 3' homology for recombination.

Future researchers will need to generate a viable *RAD23* tagging cassette, as attempts to amplify the entire cassette from a ligation reaction have failed to yield the desired product in sufficient quantities. There is proof-of-concept for this methodology working (data not shown), but the PCR process needs to be refined to reduce non-specific amplification and increase amplification of the ~7500 bp product. Once the desired

product is amplified to abundance, the suspension can be directly transformed into *Tetrahymena*.

The base plasmids created in this project—each containing a different epitope tag without any appended genes—can allow for endogenous tagging of virtually any gene by ligating the gene of interest (with ~1 kb of upstream sequence) upstream of the tagging cassette followed by the insertion of the gene's 3' NTS immediately downstream of the tagging cassette. The terminal, non-transcribed sequences provide homologous sequence required for recombination into the endogenous locus of the gene of interest.

Characterizing Rad23 in *Tetrahymena thermophila* will require elucidation of its suspected interacting partners. In yeast, two canonical binding partners of Rad23 are Rad4 and Rpn1. Since these two proteins are likely factors in connecting the proteasome to NER dynamics, verification of their potential interactions with Rad23 would show a general conservation of this regulatory axis in *Tetrahymena*, further supporting its potential as a relevant model organism in the study of GG-NER. Using the 2HA tagging construct, endogenously-expressed Rad23-2HA can be immunoprecipitated using anti-2HA antibodies. This solution could be immunoblotted to reveal suspected binding partners. The Smith laboratory has anti-Rad4 antibodies, and any gene could easily be tagged to facilitate immunoblotting using the 3XFLAG or StrepII constructs designed in this thesis. To our knowledge, there have been no reported uses of the StrepII tag in *T. thermophila*, despite its impressive utility in purification procedures. If it is shown to work effectively, this will provide the ciliate community with another useful tool to produce protists. With putative roles in regulating transcription, Rad4, Rad23, and 19S subunits could be tagged using the tagging constructs so that chromatin immunoprecipitation

followed by DNA sequencing could be performed to identify promoter elements in *T. thermophila* to which these proteins bind.

Additionally, Rad23 complexes immunoprecipitated from cells could be sent off for analysis via mass spectrometry. This precise readout will indicate the amino acid sequences of binding partners, and if there are unexpected amino acids present they can be used as a query against a database to divulge the protein to which the sequence belongs. Even more, this technique can describe the nature of ubiquitin chains on specific lysine residues. By investigating the ubiquitin profiles of the different rad23^{ubl} mutants before and after stressor conditions, a possible regulatory code could be unveiled where different chain lengths, linkages, and lysine conjugations predictably influence the interactions of Rad23, especially with the proteasome. When the *RAD23*-StrepII or *RAD23*-3XFLAG constructs are finished, the gentle elution steps these tags provide during purification will help preserve the sometimes-delicate structure of multiple post-translational modification profiles on specific protein domains.

As described above, Rad23 plays an important role as a shuttling factor for the proteasome but also associates with Rad4 in the nucleus. These roles suggest a dynamic movement of Rad23 within the cell, but there is little direct evidence of this from microscopy studies; most researchers focus solely on observing Rad23 colocalizing with damage. Using the *RAD23*-GFP construct, intracellular localization of Rad23 could be observed before and after various stressor conditions (especially UV and proteasome inhibition). Additionally, *Tetrahymena* offer the additional aspect of having two distinct nuclei: the polyploid, transcriptionally active macronucleus and the diploid, transcriptionally silent micronucleus. One would assume Rad23 would migrate primarily

to the micronucleus after UV damage as a GG-NER protein with no direct role in TC-NER, but it would be interesting to see if perhaps the transcriptional regulation via Rad23 yields contrary results. Colocalization could be performed with other proteins that have different tags, such as Rad4-RFP. The GFP in the tagging cassette of this thesis could be excised and replaced with a compatibly digested fluorescent protein, creating a cassette that only needs to be flanked by a gene of interest to facilitate endogenous tagging.

The *RAD23* knockout construct designed in this thesis can be used to delete the *T. thermophila RAD23* gene. There are currently no *rad23*Δ strains of *T. thermophila*. Downregulating expression using small-hairpin RNAs (shRNAs) could allow some residual expression of Rad23, and the shRNAs must be experimentally introduced each time a knock-down effect is desired. Studying Rad23 using ectopic expression cassettes under the control of an inducible promoter does not prevent the expression of the native gene, thus endogenous Rad23 is unaccounted for when interpreting data, leading to experimental variability.

Despite what has been completed in this project, more work remains. Aside from the above-mentioned PCR troubleshooting of the tagging cassette from a ligation reaction, a priority is the eventual sequencing of the plasmids to verify their contents. With so much lab time required between the transformation of the cassette and the actual generation of data, it is imperative that the cassettes have sequencing confirmation to ensure proper reading frames, lack of mutations, and that all desired sequences are present. Nonetheless, the tools designed in this thesis will hopefully benefit future scientists in their endeavors to characterize Rad23 in *Tetrahymena*.

REFERENCES

- Bazirgan, O. A., & Hampton, R. Y. (2005). Cdc48 – Ufd2 – Rad23 : the road less ubiquitinated? *Nature Cell Biology*, 7(3), 207–209.
- Bergink, S., & Jentsch, S. (2009). Principles of ubiquitin and SUMO modifications in DNA repair. *Nature*, 458(7237), 461–467. <https://doi.org/10.1038/nature07963>
- Bergink, S., Toussaint, W., Luijsterburg, M. S., Dinant, C., Alekseev, S., Hoeijmakers, J. H. J., ... Vermeulen, W. (2012). Recognition of DNA damage by XPC coincides with disruption of the XPC-RAD23 complex. *Journal of Cell Biology*, 196(6), 681–688. <https://doi.org/10.1083/jcb.201107050>
- Burschowsky, D., Rudolf, F., Rabut, G., Herrmann, T., Matthias, P., & Wider, G. (2011). Structural analysis of the conserved ubiquitin-binding motifs (UBMs) of the translesion polymerase iota in complex with ubiquitin. *Journal of Biological Chemistry*, 286(2), 1364–1373. <https://doi.org/10.1074/jbc.M110.135038>
- Chen, L., & Madura, K. (2002). Rad23 promotes the targeting of proteolytic substrates to the proteasome. *Molecular and Cellular Biology*, 22(13), 4902–13. <https://doi.org/10.1128/MCB.22.13.4902>
- Chen, L., Shinde, U., Ortolan, T. G., & Madura, K. (2001). Ubiquitin-associated (UBA) domains in Rad23 bind ubiquitin and promote inhibition of multi-ubiquitin chain assembly. *EMBO Reports*, 2(10), 933–938. <https://doi.org/10.1093/embo-reports/kve203>
- Chen, X., Velmurugu, Y., Zheng, G., Park, B., Shim, Y., Kim, Y., ... Min, J.-H. (2015). Kinetic gating mechanism of DNA damage recognition by Rad4/XPC. *Nature Communications*, 6, 5849. <https://doi.org/10.1038/ncomms6849>
- Cuijk, L. Van, Belle, G. J. Van, Turkyilmaz, Y., Poulsen, S. L., Janssens, R. C., Theil, A. F., ... Marteijn, J. A. (2015). SUMO and ubiquitin-dependent XPC exchange drives nucleotide excision repair. *Nature Communications*, 6(May), 1–10. <https://doi.org/10.1038/ncomms8499>
- Dantuma, N. P., Heinen, C., & Hoogstraten, D. (2009). The ubiquitin receptor Rad23: At the crossroads of nucleotide excision repair and proteasomal degradation. *DNA Repair*. <https://doi.org/10.1016/j.dnarep.2009.01.005>
- Dexheimer, T. S. (2013). DNA Repair Pathways and Mechanisms. In *DNA Repair of Cancer Stem Cells* (pp. 19–32). <https://doi.org/10.1007/978-94-007-4590-2>
- Dijk, M., Typas, D., Mullenders, L., & Pines, A. (2014). Insight in the multilevel regulation of NER. *Experimental Cell Research*, 329(1), 116–123. <https://doi.org/10.1016/j.yexcr.2014.08.010>

- El-Mahdy, M. A., Zhu, Q., Wang, Q.-E., Wani, G., Praetorius-Ibba, M., & Wani, A. A. (2006). Cullin 4A-mediated proteolysis of DDB2 protein at DNA damage sites regulates in vivo lesion recognition by XPC. *J. Biol. Chem.*, *281*(73), 13404–13411.
- Elsasser, S., Chandler-Mitilello, D., Müller, B., Hanna, J., & Finley, D. (2004). Rad23 and Rpn10 serve as alternate ubiquitin receptors for the proteasome. *Journal of Biological Chemistry*, *279*(26), 26817–26822.
<https://doi.org/10.1074/jbc.M404020200>
- Elsasser, S., & Finley, D. (2005). Delivery of ubiquitinated substrates to protein-unfolding machines. *Nature Cell Biology*, *7*(8), 742–749.
<https://doi.org/10.1038/ncb0805-742>
- Fagbemi, A., Orelli, B., & Schärer, O. D. (2011). Regulation of endonuclease activity in human nucleotide excision repair. *DNA Repair*, *10*(7), 722–729.
<https://doi.org/10.1016/j.jneumeth.2010.08.011>.Autogenic
- Ferdous, A., Sikder, D., Gillette, T., Nalley, K., Kodadek, T., & Johnston, S. A. (2007). The role of the proteasomal ATPases and activator monoubiquitylation in regulating Gal4 binding to promoters. *Genes and Development*, *21*(1), 112–123.
<https://doi.org/10.1101/gad.1493207>
- Finley, D. (2009). Recognition and processing of ubiquitin-protein conjugates by the proteasome. *Annual Review of Biochemistry*, *78*, 477–513.
<https://doi.org/10.1146/annurev.biochem.78.081507.101607>.Recognition
- Fitch, M. E., Cross, I. V., Turner, S. J., Adimoolam, S., Lin, C. X., ...Ford, J. M. (2003). The DDB2 nucleotide excision repair gene product p48 enhances global genomic repair in p53 deficient human fibroblasts. *DNA Repair*, *2*(7), 819–826.
[https://doi.org/10.1016/S1568-7864\(03\)00066-1](https://doi.org/10.1016/S1568-7864(03)00066-1)
- Fong, Y. W., Inouye, C., Yamaguchi, T., Cattoglio, C., Grubisic, I., & Tjian, R. (2011). A DNA Repair Complex Functions as an Oct4/Sox2 Coactivator in Embryonic Stem Cells. *Cell*, *147*(1), 120–131. <https://doi.org/10.1016/j.cell.2011.08.038>.A
- Fuss, J., & Tainer, J. (2011). XPB and XPD helicases in TFIIH orchestrate DNA duplex opening and damage verification to coordinate repair with transcription and cell cycle via CAK kinase, *70*(4), 646–656. <https://doi.org/10.1002/ana.22528>.Toll-like
- Gillette, T. G., Huang, W., Russell, S. J., Reed, S. H., Johnston, S. A., & Friedberg, E. C. (2001). The 19S complex of the proteasome regulates nucleotide excision repair in yeast. *Genes and Development*, *15*(12), 1528–1539.
<https://doi.org/10.1101/gad.869601>
- Gillette, T. G., Yu, S., Zhou, Z., Waters, R., Johnston, S. A., & Reed, S. H. (2006). Distinct functions of the ubiquitin-proteasome pathway influence nucleotide excision repair. *The EMBO Journal*, *25*(11), 2529–2538.
<https://doi.org/10.1038/sj.emboj.7601120>

- Glickman, M. H., Rubin, D. M., Fu, H., Larsen, C. N., Coux, O., Wefes, I., ... Finley, D. (1999). Functional analysis of the proteasome regulatory particle. *Molecular Biology Reports*, 26(1–2), 21–8. <https://doi.org/10.1023/A:1006928316738>
- Gordon, J., Harel, M., Canner, D., & Gorrell, A. (2011). Ubiquitin Structure and Function. Retrieved from http://proteopedia.org/wiki/index.php/Ubiquitin_Structure_%26_Function
- Hanania, U., Furman-Matarasso, N., Ron, M., & Avni, A. (1999). Isolation of a novel SUMO protein from tomato that suppresses EIX-induced cell death. *Plant J.*, 19(5), 533–541.
- He, J., Zhu, Q., Wani, G., Sharma, N., Han, C., Qian, J., ... Wani, A. A. (2014). Ubiquitin-specific Protease 7 Regulates Nucleotide Excision Repair through Deubiquitinating XPC Protein and Preventing XPC Protein from Undergoing Ultraviolet Light-induced and VCP/p97 Protein-regulated Proteolysis. *Journal of Biological Chemistry*, 289(39), 27278–27289. <https://doi.org/10.1074/jbc.M114.589812>
- Heinen, C., Ács, K., Hoogstraten, D., & Dantuma, N. P. (2011). C-terminal UBA domains protect ubiquitin receptors by preventing initiation of protein degradation. *Nature Communications*, 2, 191. <https://doi.org/10.1038/ncomms1179>
- Hiyama, H., Yokoi, M., Masutani, C., Sugasawa, K., Maekawa, T., Tanaka, K., ... Hanaoka, F. (1999). Interaction of hHR23 with S5a. The ubiquitin-like domain of hHR23 mediates interaction with S5a subunit of 26 S proteasome. *Journal of Biological Chemistry*, 274(39), 28019–28025. <https://doi.org/10.1074/jbc.274.39.28019>
- Hsieh, P. and Yamana, K. (2009). DNA mismatch repair: Molecular mechanism, cancer and ageing. *Mech Ageing Dev*, 129, 391–407. <https://doi.org/10.1016/j.mad.2008.02.012>.DNA
- Husnjak, K., & Dikic, I. (2012). Ubiquitin-Binding Proteins: Decoders of Ubiquitin-Mediated Cellular Functions. *Annual Review of Biochemistry*, 81(1), 291–322. <https://doi.org/10.1146/annurev-biochem-051810-094654>
- Jackson, S. P., & Durocher, D. (2013). Regulation of DNA Damage Responses by Ubiquitin and SUMO. *Molecular Cell*, 49(5), 795–807. <https://doi.org/10.1016/j.molcel.2013.01.017>
- Kamitani, T., Kito, K., Nguyen, H. P., Fukuda-Kamitani, T., & Yeh, E. T. (1998). Characterization of a second member of the sentrin family of ubiquitin-like proteins. *J. Biol. Chem.* 273, 11349–11353 (1998). *Journal of Biological Chemistry*, 273, 11349–11353.
- Kim, I., Mi, K., & Rao, H. (2004). Multiple Interactions of Rad23 Suggest a Mechanism for Ubiquitylated Substrate Delivery Important in Proteolysis IkJin. *Molecular*

- Biology of the Cell*, 15(April), 3357–3365. <https://doi.org/10.1091/mbc.E03>
- Kim, W., Bennett, E. J., Huttlin, E. L., Guo, A., Li, J., Sowa, M. E., ... Gygi, S. P. (2011). Systematic and quantitative assessment of the ubiquitin modified proteome. *Molecular Cell*, 44(2), 325–340. <https://doi.org/10.1016/j.molcel.2011.08.025>.Systematic
- Komander, D., & Rape, M. (2012). The Ubiquitin Code. *Annual Review of Biochemistry*, 81(1), 203–229. <https://doi.org/10.1146/annurev-biochem-060310-170328>
- Krzyszinski, J. Y., Choe, V., Shao, J., Bao, X., Cheng, H., Luo, S., ... Rao, H. (2014). XPC promotes MDM2-mediated degradation of the p53 tumor suppressor. *Molecular Biology of the Cell*, 25(2), 213–221. <https://doi.org/10.1091/mbc.E13-05-0293>
- Kumar, S., Talis, A. L., Peter, M., Kumar, S., Talis, A. L., & Howley, P. M. (1999). Identification of HHR23A as a Substrate for E6-associated Protein-mediated Ubiquitination. *Journal of Biological Chemistry*, 274(26), 18785–18792. <https://doi.org/10.1074/jbc.274.26.18785>
- Lambertson, D., Chen, L., & Madura, K. (1999). Pleiotropic defects caused by loss of the proteasome-interacting factors Rad23 and Rpn10 of *Saccharomyces cerevisiae*. *Genetics*, 153(1), 69–79.
- Lambertson, D., Chen, L., & Madura, K. (2003). Investigating the importance of proteasome-interaction for Rad23 function. *Curr Genet*, 42(4), 199–208. <https://doi.org/10.1007/s00294-002-0350-7>
- Li, C., Golebiowski, F., Onishi, Y., Samara, N., Sugasawa, K., & Yang, W. (2015). Tripartite DNA Lesion REcognition and Verification by XPC, TFIIH, and XPA in Nucleotide Excision Repair. *Molecular Cell*, 3(10), 973–982. [https://doi.org/10.1016/S2215-0366\(16\)30284-X](https://doi.org/10.1016/S2215-0366(16)30284-X).Epidemiology
- Liang, R. Y., Chen, L., Ko, B. T., Shen, Y. H., Li, Y. Te, Chen, B. R., ... Chuang, S. M. (2014). Rad23 interaction with the proteasome is regulated by phosphorylation of its ubiquitin-like (UbL) domain. *Journal of Molecular Biology*, 426(24), 4049–4060. <https://doi.org/10.1016/j.jmb.2014.10.004>
- Lommel, L., Ortolan, T., Chen, L., Madura, K., & Sweder, K. S. (2002). Proteolysis of a nucleotide excision repair protein by the 26S proteasome. *Current Genetics*, 42(1), 9–20. <https://doi.org/10.1007/s00294-002-0332-9>
- Lowe, E. D., Hasan, N., Trempe, J. F., Fonso, L., Noble, M. E. M., Endicott, J. A., ... Brown, N. R. (2006). Structures of the Dsk2 UBL and UBA domains and their complex. *Acta Crystallographica Section D: Biological Crystallography*, 62(2), 177–188. <https://doi.org/10.1107/S0907444905037777>
- Luijsterburg, M. S., Von Bornstaedt, G., Gourdin, A. M., Politi, A. Z., Moné, M. J.,

- Warmerdam, D. O., ... Höfer, T. (2010). Stochastic and reversible assembly of a multiprotein DNA repair complex ensures accurate target site recognition and efficient repair. *Journal of Cell Biology*, 189(3), 445–463. <https://doi.org/10.1083/jcb.200909175>
- Maganti, N., Moody, T. D., Truax, A. D., Thakkar, M., Spring, A. M., Germann, M. W., & Greer, S. F. (2014). Nonproteolytic roles of 19S ATPases in transcription of CIITApIV genes. *PLoS ONE*, 9(3). <https://doi.org/10.1371/journal.pone.0091200>
- Marteijn, J. a, Lans, H., Vermeulen, W., & Hoeijmakers, J. H. J. (2014). Understanding nucleotide excision repair and its roles in cancer and ageing. *Nature Reviews. Molecular Cell Biology*, 15(7), 465–81. <https://doi.org/10.1038/nrm3822>
- Miele, A., Bystricky, K., & Dekker, J. (2009). Yeast silent mating type loci form heterochromatic clusters through silencer protein-dependent long-range interactions. *PLoS Genetics*, 5(5). <https://doi.org/10.1371/journal.pgen.1000478>
- Myung, J., Kim, K. B., & Crews, C. M. (2001). The ubiquitin-proteasome pathway and proteasome inhibitors. *Medicinal Research Reviews*, 21(4), 245–73. <https://doi.org/10.1016/j.biotechadv.2011.08.021>. Secreted
- Ng, J. M. Y., Vrieling, H., Sugasawa, K., Ooms, M. P., Grootegoed, J. A., Vreeburg, J. T. M., ... van der Horst, G. T. J. (2002). Developmental defects and male sterility in mice lacking the ubiquitin-like DNA repair gene mHR23B. *Molecular and Cellular Biology*, 22(4), 1233–1245. <https://doi.org/10.1128/MCB.22.4.1233-1245.2002>
- Nie, M., Aslanian, A., Prudden, J., Heideker, J., Vashisht, A. A., Wohlschlegel, J. A., ... Boddy, M. N. (2012). Dual recruitment of Cdc48 (p97)-Ufd1-Npl4 ubiquitin-selective segregase by small ubiquitin-like modifier protein (SUMO) and ubiquitin in SUMO-targeted ubiquitin ligase-mediated genome stability functions. *Journal of Biological Chemistry*, 287(35), 29610–29619. <https://doi.org/10.1074/jbc.M112.379768>
- Nishi, R., Alekseev, S., Dinant, C., Hoogstraten, D., Houtsmuller, A. B., Hoeijmakers, J. H. J., ... Sugasawa, K. (2009). UV-DDB-dependent regulation of nucleotide excision repair kinetics in living cells. *DNA Repair*, 8(6), 767–776. <https://doi.org/10.1016/j.dnarep.2009.02.004>
- Ortolan, T. G., Chen, L., Tongaonkar, P., & Madura, K. (2004). Rad23 stabilizes Rad4 from degradation by the Ub/proteasome pathway. *Nucleic Acids Research*, 32(22), 6490–6500. <https://doi.org/10.1093/nar/gkh987>
- Ortolan, T. G., Tongaonkar, P., Lambertson, D., Chen, L., Schaubert, C., & Madura, K. (2000). The DNA repair protein rad23 is a negative regulator of multi-ubiquitin chain assembly. *Nature Cell Biology*, 2(9), 601–8. <https://doi.org/10.1038/35023547>
- Peng, J., Schwartz, D., Elias, J. E., Thoreen, C. C., Cheng, D., Marsischky, G., ... Gygi, S. P. (2003). A proteomics approach to understanding protein ubiquitination. *Nature*

Biotechnology, 21 VN-r(8), 921–926. <https://doi.org/10.1038/nbt849>

- Poulsen, S. L., Hansen, R. K., Wagner, S. A., van Cuijk, L., van Belle, G. J., Streicher, W., ... Mailand, N. (2013). RNF111/Arkadia is a SUMO-targeted ubiquitin ligase that facilitates the DNA damage response. *The Journal of Cell Biology*, 201(6), 797–807. <https://doi.org/10.1083/jcb.201212075>
- Puumalainen, M.-R., Lessel, D., Rütthemann, P., Kaczmarek, N., Bachmann, K., ... Naegeli, H. (2014). Chromatin retention of DNA damage sensors DDB2 and XPC through loss of p97 segregase causes genotoxicity. *Nature Communications*, 5. <https://doi.org/10.1038/ncomms4695>
- Raasi, S., Orlov, I., Fleming, K. G., & Pickart, C. M. (2004). Binding of polyubiquitin chains to ubiquitin-associated (UBA) domains of HHR23A. *Journal of Molecular Biology*, 341(5), 1367–1379. <https://doi.org/10.1016/j.jmb.2004.06.057>
- Ramsey, K. L., Smith, J. J., Dasgupta, A., Maqani, N., Grant, P., & Auble, D. T. (2004). The NEF4 Complex Regulates Rad4 Levels and Utilizes Snf2 / Swi2-Related ATPase Activity for Nucleotide Excision Repair. *Molecular and Cellular Biology*, 24(14), 6362–6378. <https://doi.org/10.1128/MCB.24.14.6362>
- Reed, S. H., & Gillette, T. G. (2007). Nucleotide excision repair and the ubiquitin proteasome pathway-Do all roads lead to Rome? *DNA Repair*. <https://doi.org/10.1016/j.dnarep.2006.10.026>
- Richly, H., Rape, M., Braun, S., Rumpf, S., Hoegge, C., & Jentsch, S. (2005). A series of ubiquitin binding factors connects CDC48/p97 to substrate multiubiquitylation and proteasomal targeting. *Cell*, 120(1), 73–84. <https://doi.org/10.1016/j.cell.2004.11.013>
- Rosenzweig, R., Bronner, V., Zhang, D., Fushman, D., & Glickman, M. H. (2012). Rpn1 and Rpn2 coordinate ubiquitin processing factors at proteasome. *Journal of Biological Chemistry*, 287(18), 14659–14671. <https://doi.org/10.1074/jbc.M111.316323>
- Saeki, Y. (2017). Ubiquitin recognition by the proteasome. *Journal of Biochemistry*, 161(2), 113–124. <https://doi.org/10.1093/jb/mvw091>
- Saeki, Y., Saitoh, A., Toh-e, A., & Yokosawa, H. (2002). Ubiquitin-like proteins and Rpn10 play cooperative roles in ubiquitin-dependent proteolysis. *Biochemical and Biophysical Research Communications*, 293(3), 986–992. [https://doi.org/10.1016/S0006-291X\(02\)00340-6](https://doi.org/10.1016/S0006-291X(02)00340-6)
- Schärer, O. D. (2013). Nucleotide Excision Repair in Eukaryotes. *Cold Spring Harb Perspect Biol*, 1–19.
- Schmidt, M., Hanna, J., Elsasser, S., & Finley, D. (2005). Proteasome-associated proteins: Regulation of a proteolytic machine. *Biological Chemistry*, 386(8), 725–

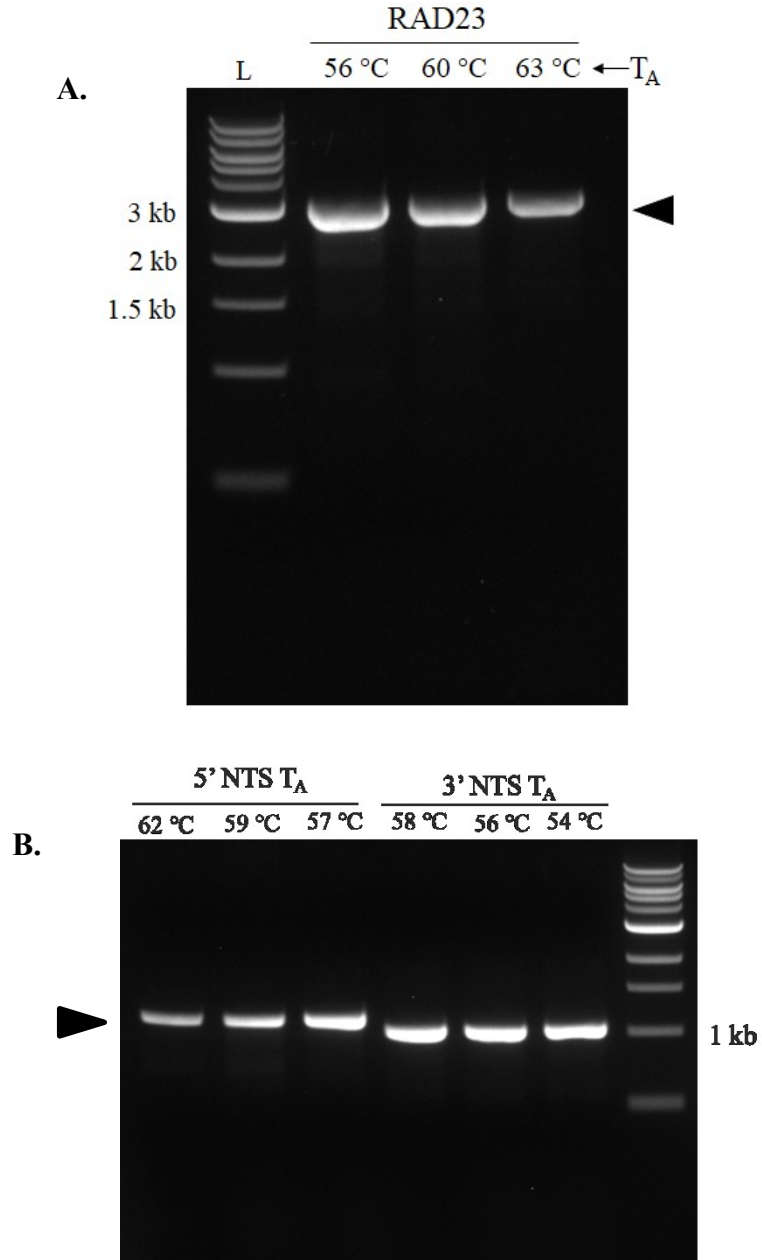
737. <https://doi.org/10.1515/BC.2005.085>

- Shi, Y., Chen, X., Elsasser, S., Stocks, B. B., Tian, G., Lee, B.-H., ... Walters2, and K. J. (2016). Rpn1 provides adjacent receptor sites for substrate binding and deubiquitination by the proteasome. *Science*, *12*(6), 403–409. <https://doi.org/10.1016/j.jamda.2011.04.014>. Sarcopenia
- Sugasawa, K. (2016). Molecular mechanisms of DNA damage recognition for mammalian nucleotide excision repair. *DNA Repair*, *44*, 110–117. <https://doi.org/10.1016/j.dnarep.2016.05.015>
- Sugasawa, K., Okamoto, T., Shimizu, Y., Masutani, C., Iwai, S., & Hanaoka, F. (2001). A multistep damage recognition mechanism for global genomic nucleotide excision repair. *Genes and Development*, *15*(5), 507–521. <https://doi.org/10.1101/gad.866301>
- Sugasawa, K., Okuda, Y., Saijo, M., Nishi, R., Matsuda, N., Chu, G., ... Hanaoka, F. (2005). UV-induced ubiquitylation of XPC protein mediated by UV-DDB-ubiquitin ligase complex. *Cell*, *121*(3), 387–400. <https://doi.org/10.1016/j.cell.2005.02.035>
- Tsuchiya, H., Ohtake, F., Arai, N., Kaiho, A., Yasuda, S., Tanaka, K., & Saeki, Y. (2017). In Vivo Ubiquitin Linkage-type Analysis Reveals that the Cdc48-Rad23/Dsk2 Axis Contributes to K48-Linked Chain Specificity of the Proteasome. *Molecular Cell*, *66*(4), 488–502.e7. <https://doi.org/10.1016/j.molcel.2017.04.024>
- Varadan, R., Assfalg, M., Raasi, S., Pickart, C., & Fushman, D. (2005). Structural determinants for selective recognition of a Lys48-linked polyubiquitin chain by a UBA domain. *Molecular Cell*, *18*(6), 687–698. <https://doi.org/10.1016/j.molcel.2005.05.013>
- Wade, S. L., Poorey, K., Bekiranov, S., & Auble, D. T. (2009). The Snf1 kinase and proteasome-associated Rad23 regulate UV-responsive gene expression. *Embo J*, *28*(19), 2919–2931. <https://doi.org/10.1038/emboj.2009.229>
- Xie, Z., Liu, S., Zhang, Y., & Wang, Z. (2004). Roles of Rad23 protein in yeast nucleotide excision repair. *Nucleic Acids Research*, *32*(20), 5981–5990. <https://doi.org/10.1093/nar/gkh934>
- Zhou, Z., Humphries, N., Van Eijk, P., Waters, R., Yu, S., Kraehenbuehl, R., ... Reed, S. H. (2015). UV induced ubiquitination of the yeast Rad4-Rad23 complex promotes survival by regulating cellular dNTP pools. *Nucleic Acids Research*, *43*(15), 7360–7370. <https://doi.org/10.1093/nar/gkv680>

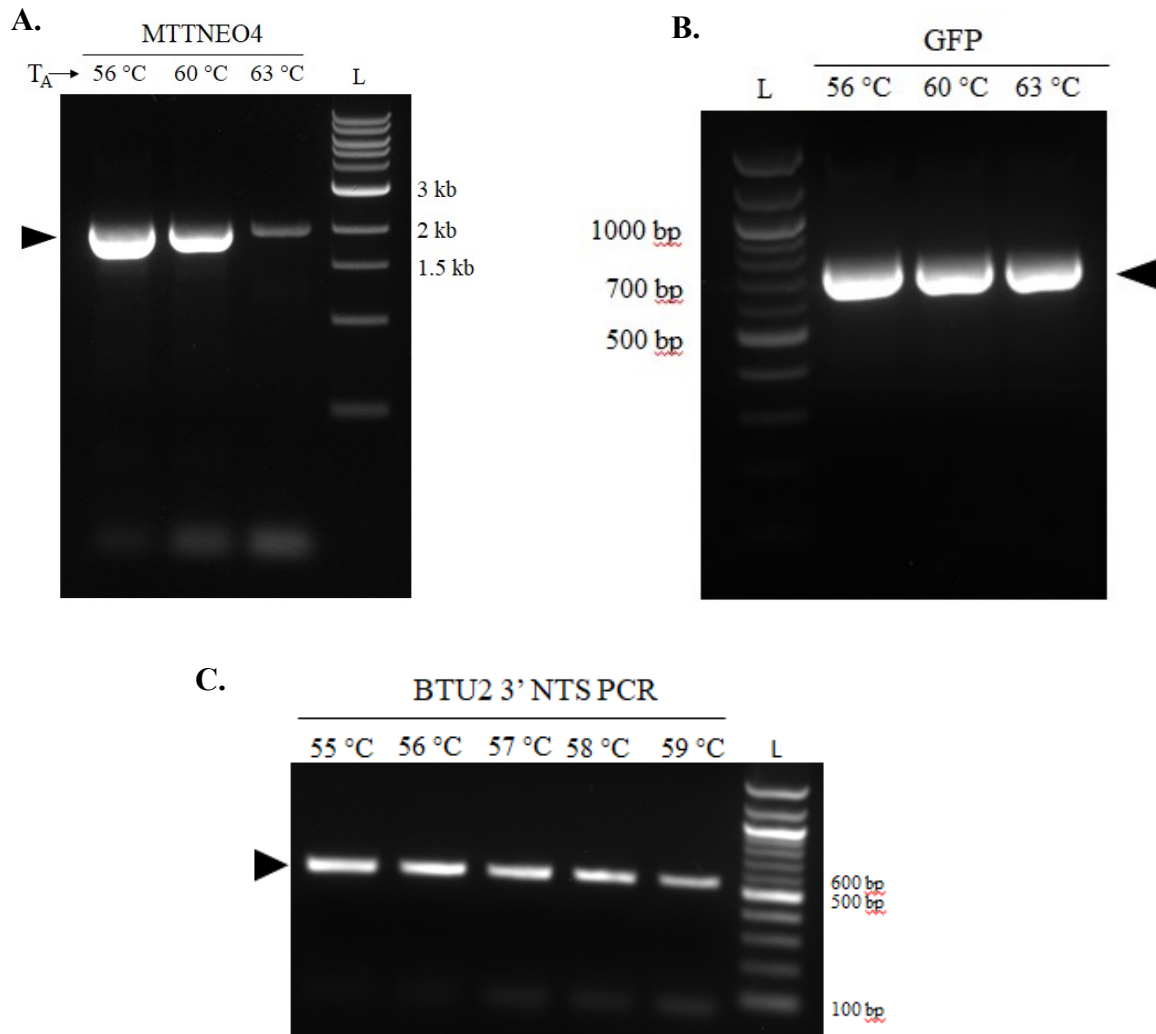
APPENDICES

Appendix A: Optimization of PCR primers

PCR was performed in order to generate the different inserts that were to be ligated into plasmids for cloning. Primers were ordered from Integrated DNA Technologies® (IDT) and optimized by using a gradient of different annealing temperatures. The annealing temperature that generated the most product with the least amount of background was chosen as the annealing temperature to be used during the copious amplification that occurred before digesting the products. A1 shows the RAD23 genomic sequence, 5'NTS, and 3'NTS optimization gels. A2 shows the optimization gels of BTU2 3'NTS, GFP, and MTTNEO4.



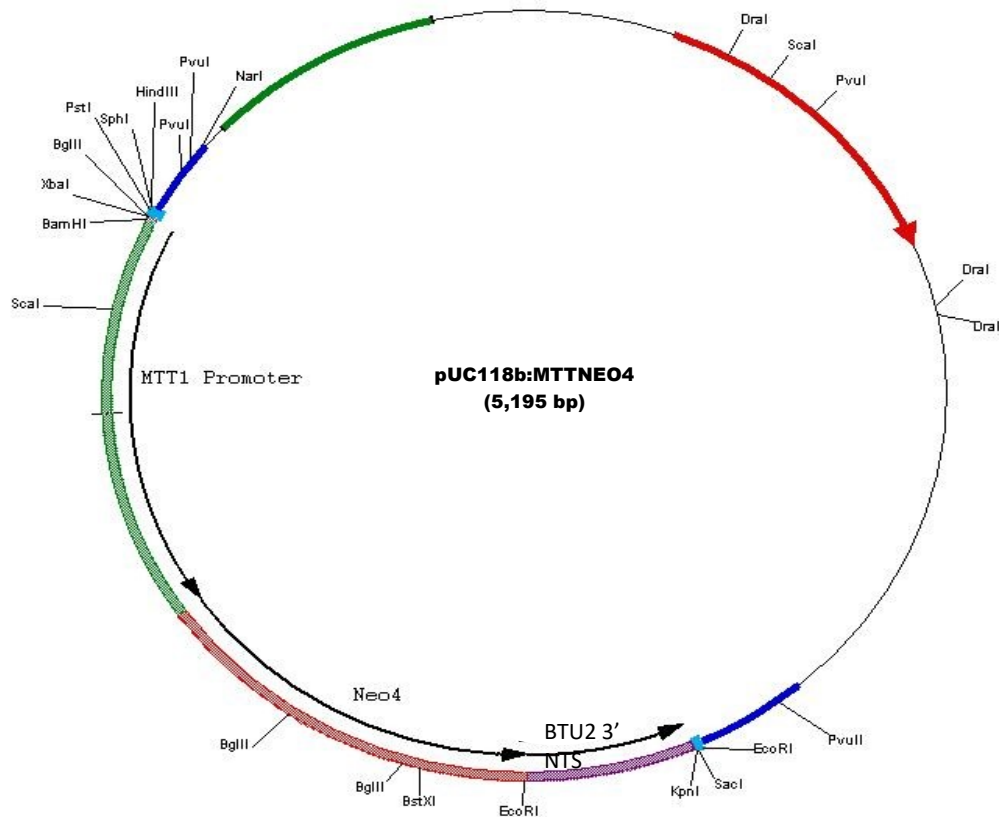
Appendix A-1. Optimization of RAD23 primers. (A) Temperatures used to optimize the primers amplifying the genomic RAD23 sequence. The arrow indicates the bands of RAD23. (B) Temperatures used to amplify the RAD23 5'NTS (lanes 1-3) and the RAD23 3'NTS (Lanes 4-6). The bands of significance are shown by the black arrow. The furthest right lane is the NEB 1kb ladder.



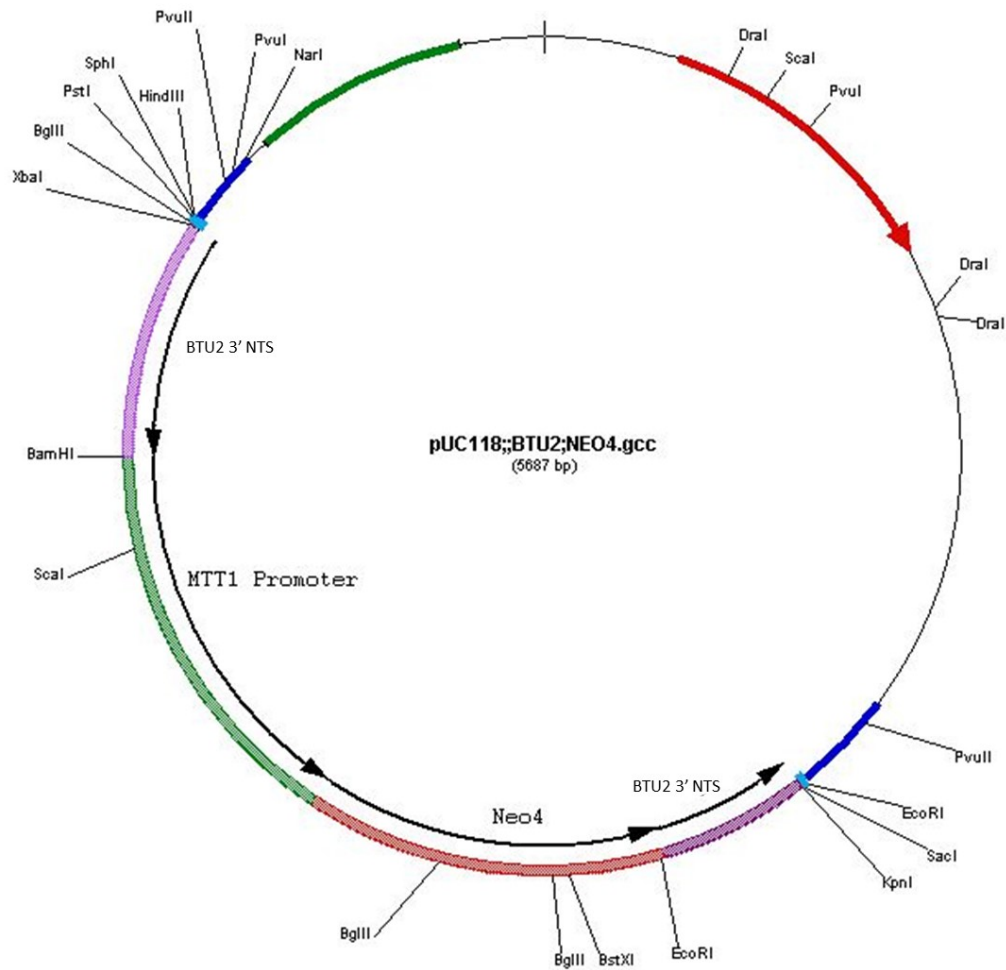
Appendix A-2. Optimization of cloning inserts used in construction of tagging vector. (A) MTTNEO4 optimization gel, with 56 °C being the chosen annealing temperature due to the highest amount of amplification. (B) Amplification of the GFP tag; 56 °C was used as the annealing temperature during the construction of the vectors. (C) The amplification of the BTU2 3' NTS; 55 °C was the chosen annealing temperature.

Appendix B: Plasmid Maps

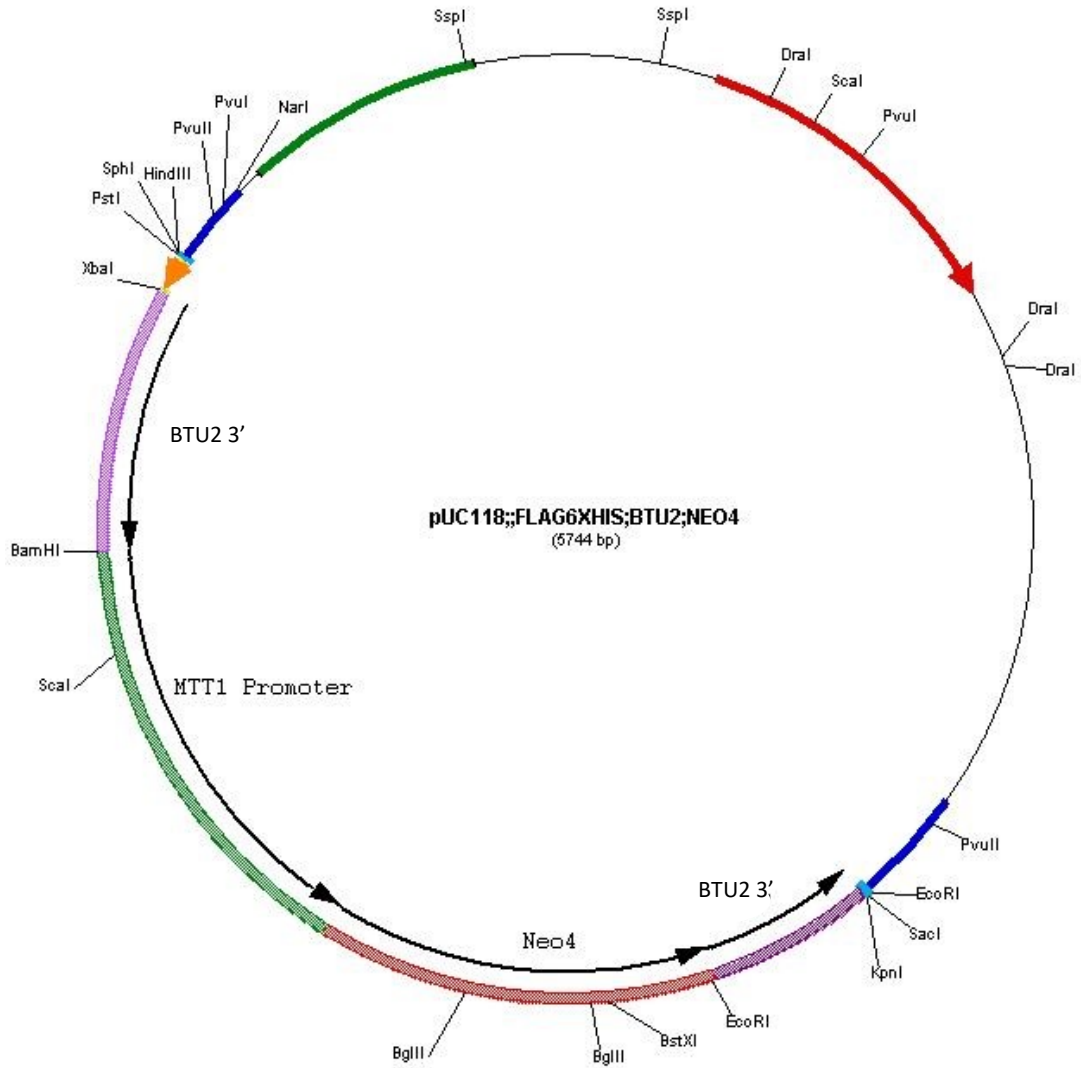
Before beginning the process of cloning, all of the vectors made in this study were designed *in silico* using Gene Construction Kit®. The following maps show the plasmids made in this study as they would appear in the software. These maps were used to generate predicted RFLP patterns during the diagnostic digests of the plasmids for screening of positive transformants.



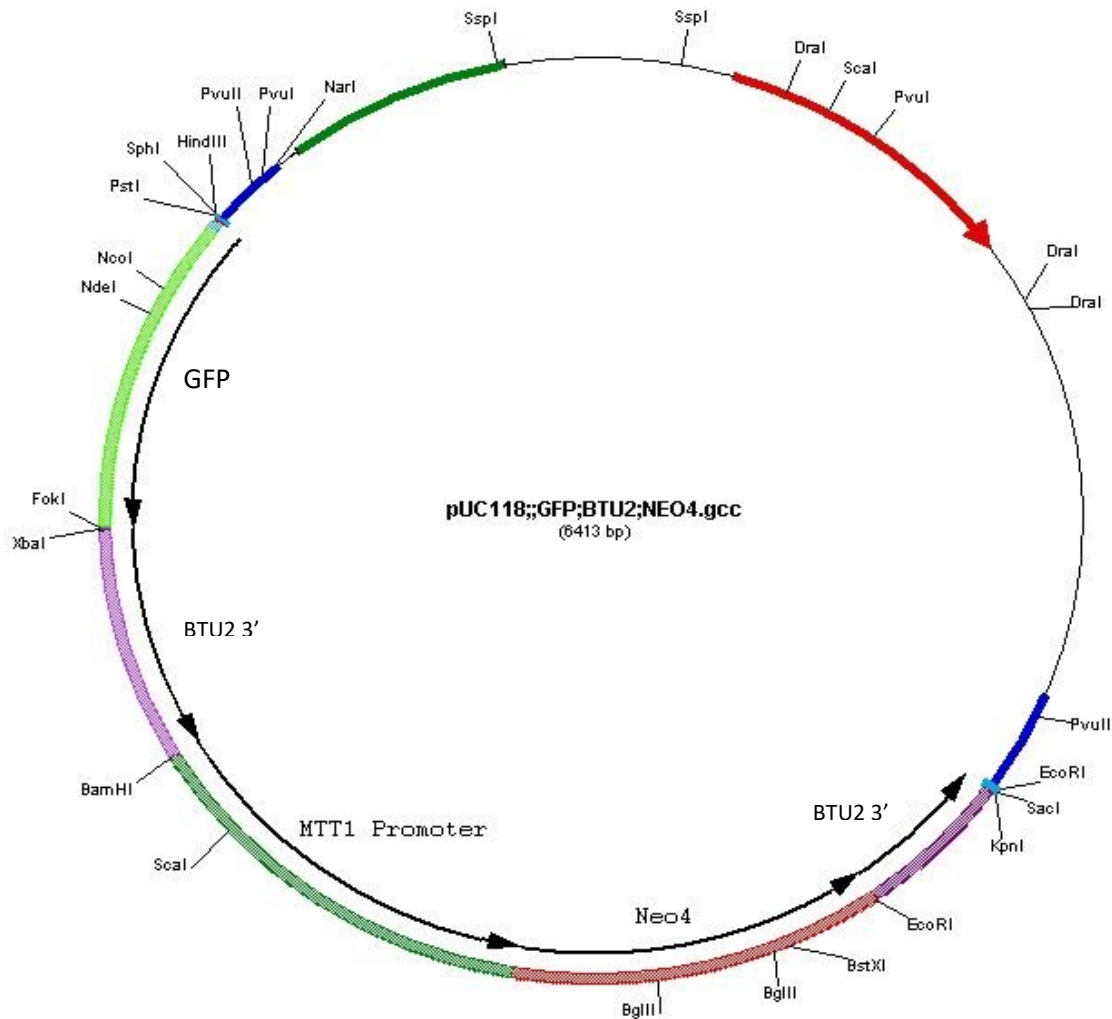
Appendix B-1. Plasmid map of pUC118b containing the MTTNEO4 cassette, generated using Gene Construction Kit. The pUC118b backbone consists of two multiple cloning sites (MCS), shown in light blue; the dark blue bars flanking the cassette represent the disrupted LacZ gene; ampicillin resistance gene is represented by the red arrow; f1 replication origin is shown as the solid green bar; the MTT1 promoter (inducible by CdCl₂) is shown in light green; the *Tetrahymena thermophila* codon-optimized paromomycin resistance gene is shown in light red; the BTU2 3' NTS (containing a poly-adenylation signal) is shown in purple. Black arrows indicate the direction of transcription.



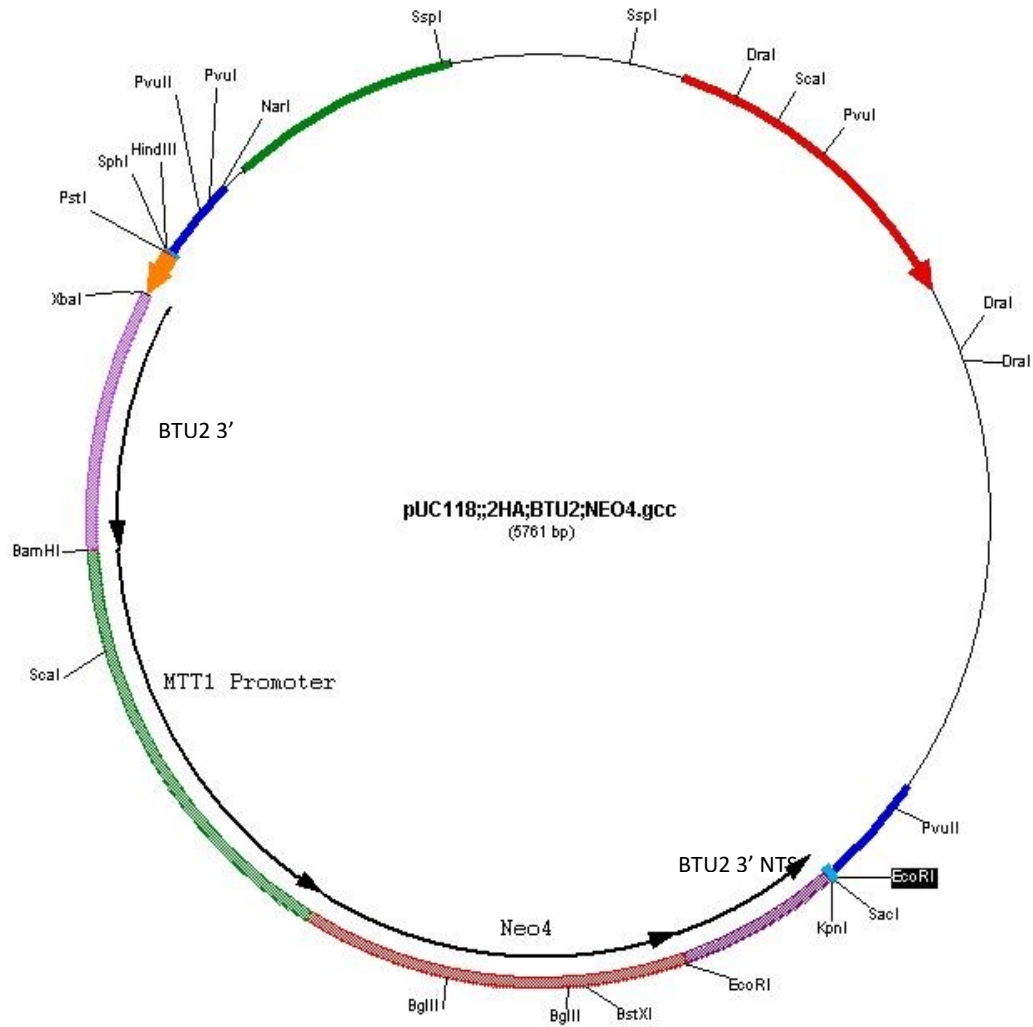
Appendix B-2. Plasmid map of pUC118b containing the MTTNEO4 cassette and BTU2 3'NTS generated using Gene Construction Kit. The pUC118b backbone consists of two multiple cloning sites (MCS), shown in light blue; the dark blue bars flanking the cassette represent the disrupted LacZ gene; ampicillin resistance gene is represented by the red arrow; f1 replication origin is shown as the solid green bar; the MTT1 promoter (inducible by CdCl₂) is shown in light green; the *Tetrahymena thermophila* codon-optimized paromomycin resistance gene is shown in light red; the BTU2 3' NTS (containing a polyadenylation signal) is shown in purple. Black arrows indicate the direction of transcription.



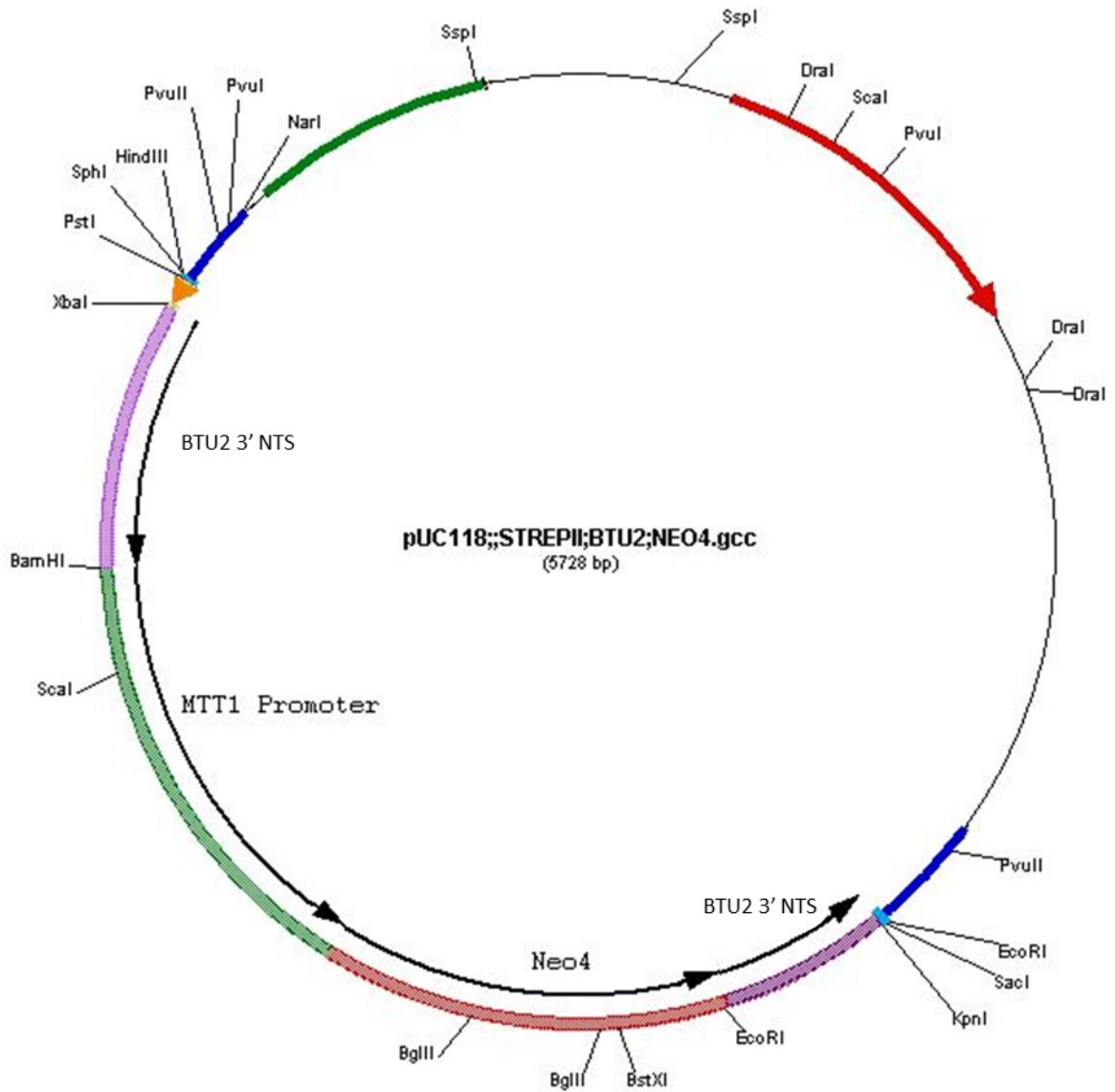
Appendix B-3. Plasmid map of pUC118b containing the MTTNEO4 cassette, BTU2 3'NTS, and 3XFLAG affinity tag generated using Gene Construction Kit. The pUC118b backbone consists of two multiple cloning sites (MCS), shown in light blue; the dark blue bars flanking the cassette represent the disrupted LacZ gene; ampicillin resistance gene is represented by the red arrow; fl replication origin is shown as the solid green bar; the MTT1 promoter (inducible by CdCl₂) is shown in light green; the *Tetrahymena thermophila* codon-optimized paromomycin resistance gene is shown in light red; the BTU2 3' NTS (containing a poly-adenylation signal) is shown in purple; the 3XFLAG coding sequence is represented as the (short) orange arrow. Black arrows indicate the direction of transcription.



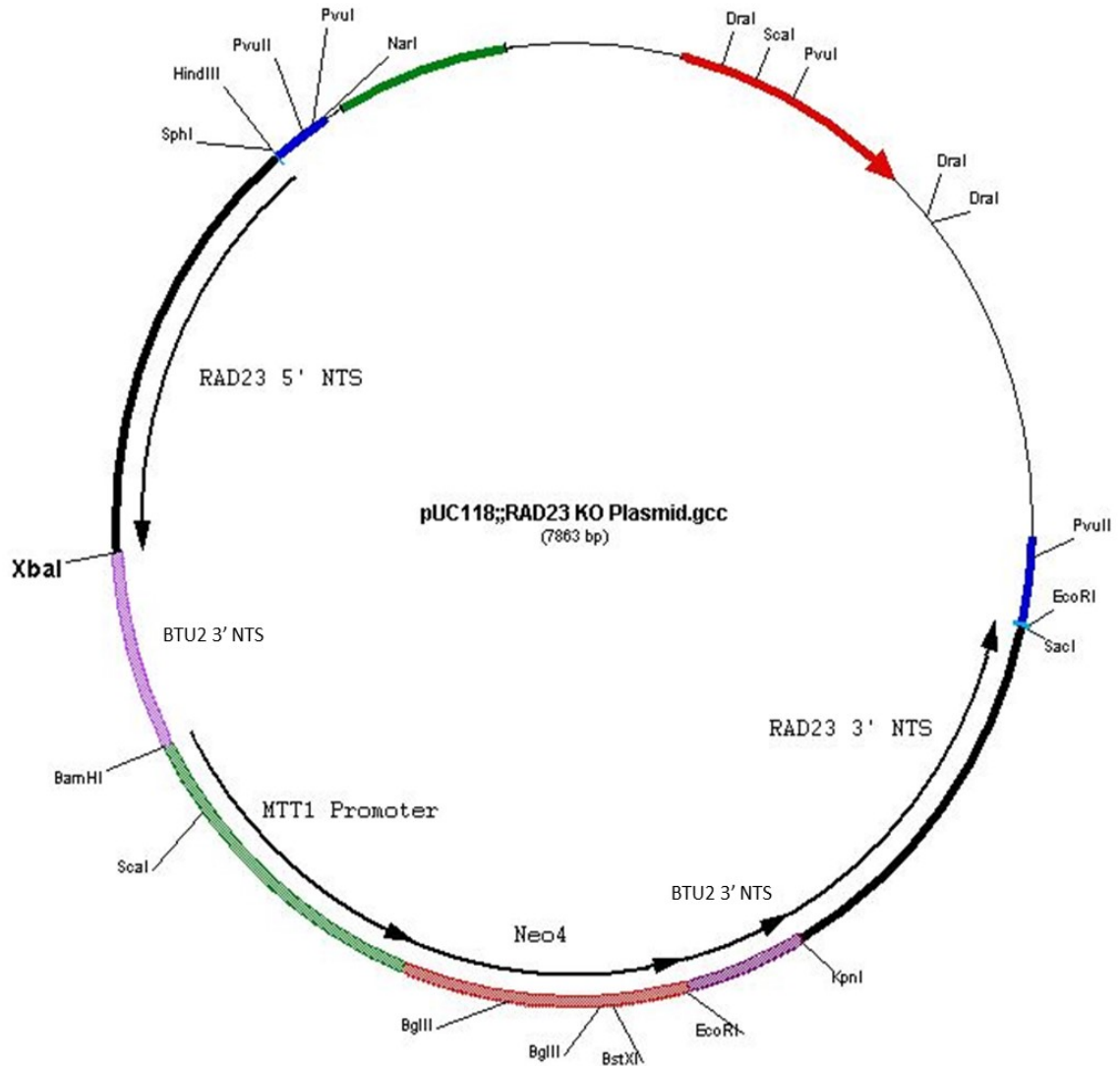
Appendix B-4. Plasmid map of pUC118b containing the MTTNEO4 cassette, generated using Gene Construction Kit. The pUC118b backbone consists of two multiple cloning sites (MCS), shown in light blue; the dark blue bars flanking the MTTNEO4 cassette represent the disrupted LacZ gene; ampicillin resistance gene is represented by the red arrow; f1 replication origin is shown as the solid green bar; the MTT1 promoter (inducible by CdCl₂) is shown in light green; the *Tetrahymena thermophila* codon-optimized paromomycin resistance gene is shown in light red; the BTU2 3' NTS (containing a polyadenylation signal) is shown in purple; the GFP coding sequence is shown in light green. Black arrows indicate the direction of transcription.



Appendix B-5. Plasmid map of pUC118b containing the MTTNEO4 cassette, generated using Gene Construction Kit. The pUC118b backbone consists of two multiple cloning sites (MCS), shown in light blue; the dark blue bars flanking the MTTNEO4 cassette represent the disrupted LacZ gene; ampicillin resistance gene is represented by the red arrow; f1 replication origin is shown as the solid green bar; the MTT1 promoter (inducible by CdCl₂) is shown in light green; the *Tetrahymena thermophila* codon-optimized paromomycin resistance gene is shown in light red; the BTU2 3' NTS (containing a polyadenylation signal) is shown in purple; the 2HA coding sequence is represented as the (short) orange arrow. Black arrows indicate the direction of transcription.



Appendix B-6. Plasmid map of pUC118b containing the MTTNEO4 cassette, generated using Gene Construction Kit. The pUC118b backbone consists of two multiple cloning sites (MCS), shown in light blue; the dark blue bars flanking the MTTNEO4 cassette represent the disrupted LacZ gene; ampicillin resistance gene is represented by the red arrow; f1 replication origin is shown as the solid green bar; the MTT1 promoter (inducible by CdCl₂) is shown in light green; the *Tetrahymena thermophila* codon-optimized paromomycin resistance gene is shown in light red; the BTU2 3' NTS (containing a polyadenylation signal) is shown in purple; the StrepII coding sequence is represented as the (short) orange arrow. Black arrows indicate the direction of transcription.



Appendix B-7. Plasmid map of pUC118b containing the MTTNEO4 cassette, generated using Gene Construction Kit. The pUC118b backbone consists of two multiple cloning sites (MCS), shown in light blue; the dark blue bars flanking the MTTNEO4 cassette represent the disrupted LacZ gene; ampicillin resistance gene is represented by the red arrow; fl replication origin is shown as the solid green bar; the MTT1 promoter (inducible by CdCl₂) is shown in light green; the *Tetrahymena thermophila* codon-optimized paromomycin resistance gene is shown in light red; the BTU2 3' NTS (containing a polyadenylation signal) is shown in purple; the RAD23 5' and 3' NTS are shown as black bars and will facilitate the insertion of the KO cassette into the endogenous RAD23 loci of *Tetrahymena thermophila*. Black arrows indicate the direction of transcription.